Geological, physical, and chemical characteristics of seafloor hydrothermal vent fields*

ZENG Zhigang[1, 2, 3, 4, **], CHEN Zuxing[1, 4], ZHANG Yuxiang[1, 4], LI Xiaohui[1, 4]

[1] Seafloor Hydrothermal Activity Laboratory, CAS Key Laboratory of Marine Geology and Environment, Institute of Oceanology, Chinese Academy of Sciences, Qingdao 266071, China

[2] Laboratory for Marine Mineral Resources, Qingdao National Laboratory for Marine Science and Technology, Qingdao 266061, China

[3] University of Chinese Academy of Sciences, Beijing 100049, China

[4] Center for Ocean Mega-Science, Chinese Academy of Sciences, Qingdao 266071, China

Abstract   Seafloor hydrothermal vent fields (SHVFs) are located in the mid-ocean ridge (MOR), back-arc basin (BAB), island arc and hot-spot environments and hosted mainly by ultramafic, mafic, felsic rocks, and sediments. The hydrothermal vent fluids of SHVFs have low oxygen, abnormal pH and temperature, numerous toxic compounds, and inorganic energy sources, such as sulfuric compounds, methane, and hydrogen. The geological, physical, and chemical characteristics of SHVFs provide important clues to understanding the formation and evolution of seafloor hydrothermal systems, leading to the determination of metal sources and the reconstruction of the physicochemical conditions of metallogenesis. Over the past two decades, we studied the geological settings, volcanic rocks, and hydrothermal products of SHVFs and drawn new conclusions in these areas, including: 1) the hydrothermal plumes in the Okinawa Trough are affected by the Kuroshio current; 2) S and Pb in the hydrothermal sulfides from MOR are mainly derived from their host igneous rocks; 3) Re and Os of vent fluids are more likely to be incorporated into Fe- and Fe-Cu sulfide mineral facies, and Os is enriched under low-temperature (<200°C) hydrothermal conditions in global SHVFs; 4) compared with low-temperature hydrothermal sulfides, sulfates, and opal minerals, high-temperature hydrothermal sulfides maintain the helium (He) isotopic composition of the primary vent fluid; 5) relatively low temperature (<116°C), oxygenated, and acidic environment conditions are favorable for forming a native sulfur chimney, and a "glue pudding" growth model can be used to understand the origin of native sulfur balls in the Kueishantao hydrothermal field; and 6) boron isotope from hydrothermal plumes and fluids can be used to describe their diffusive processes. The monitoring and understanding of the physical structure, chemical composition, geological processes, and diverse organism of subseafloor hydrothermal systems will be a future hot spot and frontier of submarine hydrothermal geology.

Keyword: vent fields; hydrothermal products; volcanic rocks; vent organisms; seafloor hydrothermal systems

1 INTRODUCTION

Seafloor hydrothermal vent fields (SHVFs) contain diverse vent fluids, hydrothermal sulfide deposits, hydrothermal plumes, metalliferous sediments, biological species. Volcanic rocks create a hydrothermal environment with alterations involving components of geological, physical, chemical, and biological variations (Hannington et al., 2005; Zeng, 2011; Humphris and Klein, 2018). Hydrothermal sulfide deposits with vent fluids, hydrothermal plumes, metalliferous sediments, biological species, and volcanic rocks provide new windows for understanding subseafloor fluid and magma processes,

as well as the impact of seafloor hydrothermal activities on seawater, sediment, and ecological environments (Von Damm, 1995; Glasby and Notsu, 2003; Hrischeva et al., 2007; Zeng et al., 2017a).

Material transport and heat budget processes of seafloor hydrothermal activities in SHVFs and the associated controlling mechanism for forming hydrothermal products (HPs) (e.g., vent fluid, hydrothermal plumes, hydrothermal sulfides, metalliferous sediments, altered volcanic rocks, organisms) remain unclear. Subseafloor fluid circulation and its physical and chemical variations are not well recognized (Tivey, 2007; Humphris and Klein, 2018). For example, the quantitative impacts of fault structure, magmatism, fluid-rock interaction, sediment, and seawater on the formation and preservation of HPs and environments remain poorly understood and the subseafloor structure and material composition of SHVFs are unconstrained, which seriously restricts the determination of the formation mechanism and fluid conditions of HPs, ecological environment, and the potential of biology resources. Shallow (<1 m), medium (1–10 m), and deep (>10 m) drilling and sampling campaigns with hydrothermal cycle modeling should be carried out in SHVFs to (I) investigate global subseafloor hydrothermal mineralization (e.g., Petersen et al., 2005, 2014), (II) study subseafloor hydrothermal systems and their constraints and effect on HPs, seawater, rock, and ecological environment, (III) determine the ore-forming mechanism of subseafloor hydrothermal sulfide deposits, and (IV) provide scientific support for understanding subseafloor biological processes and ways to protect the seafloor hydrothermal environment. These broad-scale findings are expected to provide accurate insights into subseafloor hydrothermal systems worldwide.

In this paper, we summarize major research advances concerning volcanic rocks, vent fluids, hydrothermal plumes, hydrothermal sulfides, hydrothermal alteration, oxyhydroxide, metalliferous sediment, organic matter, hydrothermal organism, and shallow water hydrothermal activity as a reference for understanding the geological, physical, and chemical characteristics of SHVFs.

2 GEOLOGICAL SETTINGS OF THE SHVFS

SHVFs are located on mid-ocean ridges (MORs), back-arc basins (BABs), island arcs (IAs) and hot-spots, which are hosted mainly by ultramafic, mafic, and felsic rocks, and sediments (Zeng et al., 2010a, 2014a, 2015a, b).

2.1 East Pacific Rise between 12°N and 13°N

The East Pacific Rise (EPR) between 12°N and 13°N is a fast-spreading ridge (10–12 cm/a) located at the boundary of the Pacific plate and Cocos plate with axial graben, marginal high, and seamount. The bathymetry changes symmetrically and becomes gradually deeper from the middle to either sides (Hékinian et al., 1983). Fresh basaltic lava have filled in the faults and fissures near the axial grabens (Gente et al., 1986). SHVFs in the EPR are hosted by mid-ocean ridge basalts (MORBs) and distributed in the axial grabens, marginal high, and southeast seamount with highly developed faults (Fouquet et al., 1996).

2.2 Mid-Atlantic Ridge

The slow-spreading Mid-Atlantic Ridge (MAR) is divided into the North MAR (NMAR) and South MAR (SMAR). At the Atlantic-Indian Ridge near 54°S, the SMAR turns and crosses the Crozet Plateau, which continues westwards to the Scotia Ridge and eastwards to the Southwest Indian Ridge (SWIR). SHVFs in the SMAR are hosted by MORBs, where the spreading rate is approximately 3.4 cm/a (DeMets et al., 1994).

The hydrothermal sulfide deposits in the Logatchev hydrothermal field (LHF) of the NMAR are mainly hosted by serpentinized harzburgite and dunite, gabbronorite, basalt, and pelagic sediments (Rouxel et al., 2004; Petersen et al., 2009; Zeng et al., 2014a, 2015a, b).

2.3 Indian Ocean Ridge

The Indian Ocean Ridges include the Central Indian Ridge (CIR), SWIR, southeast Indian Ridge (SEIR), and northwest Indian Ridge (NWIR). For example, the SWIR located between 45°E and 70°E and 26°S and 40°S stretches from Bouvet Triple Junction to the Rodriguez Triple Junction and is a super-slow spreading ridge (<2 cm/a) that acts as the main boundary between the African and Antarctica plates (Suo et al., 2017). The SWIR is approximately 8 000 km long with an oceanic crust thickness of 3.0 to 6.0 km (Muller et al., 1999). The volcanic rocks in the SWIR mainly consist of peridotite, gabbro, and basalt, and the axial rifts and limbs of SWIR are covered with thick sediment (>10 m). SHVFs located in the CIR, SWIR, and NWIR. For example, the Kairei

hydrothermal vent field in the CIR is hosted by basalt that is adjacent to mafic-, ultramafic olivine-rich rocks, and the hydrothermal fluids interact with and circulate through ultramafic rocks (Nakamura et al., 2009). Numerous hydrothermal fields were discovered in the SWIR, including the Duanqiao-1, Yuhuang-1, and Longqi-1 (Tao et al., 2014; Liao et al., 2019). The hydrothermal fluids in the Longqi-1 active vent field in the SWIR undergo a long reaction path involving both mafic and ultramafic lithologies (Tao et al., 2020).

2.4 Back-arc basins

2.4.1 Okinawa Trough

The Okinawa Trough (OT) is located in the western Ryukyu arc-trench system and extends from northeast of Taiwan, China, to southwest of Kyushu. The OT developed on the eastern edge of the Eurasian continental lithosphere and is a nascent BAB in the western Pacific. The OT is characterized by the development of normal faulting of transitional crust (atypical crust with mantle-derived material), extremely high heat flow values (up to 400–600 mW/m^2; Yamano et al., 1989) and frequent magma intrusions (includes basic to silicic magmas), which provides a favorable geological environment for the development of seafloor hydrothermal sulfides in SHVFs (Sibuet et al., 1998; Ishibashi et al., 2015). The OT is divided by the Tokara and Kerama faults into northern (NOT), middle (MOT), southern (SOT) sections (Shinjo and Kato, 2000), and the topography changes remarkably from the MOT to SOT.

By 2016, at least 15 SHVFs have been reported in the OT based on the InterRidge data base, including the Minami-Ensei, Iheya North, Clam, Jade, Hakurei, Hatoma, Yonaguni Knoll IV, and Tangyin hydrothermal vent fields (Zeng et al., 2017a). The Iheya North knoll hydrothermal field located in the Iheya North knoll volcanic complex in the MOT has a water depth of approximately 1 000 m and is hosted by pumiceous volcanic clasts, hemipelagic sediments, and hydrothermally altered volcanogenic breccias (Ishibashi et al., 2015). The Clam hydrothermal field is located in a small depression on the northern slope along the eastern part of the Iheya Ridge in the MOT (Ishibashi et al., 2015). The Yonaguni Knoll IV hydrothermal field is situated in an elongated valley with dimensions of approximately 1 000 m×500 m and mostly covered by sediment, except for the northern slope and active SHVF (Suzuki et al., 2008). The Tangyin hydrothermal field is located on the top of the Yuhua Hill seamount and is hosted by a felsic

volcanic basement with patches of sediment adjacent to a submarine canyon (Zeng et al., 2017a).

2.4.2 Eastern Manus Basin

In the eastern Manus Basin (EMB), volcanic ridges located within a remnant of island-arc crust. Lavas erupted along the ridges have variable composition including a complete series from basalt to rhyolite (Binns and Scott, 1993; Sinton et al., 2003; Hannington et al., 2005).

There are four SHVFs in or near the volcanic ridges in the EMB: the PACMANUS, DESMOS caldera, Susu Knolls, and Solwara 12 hydrothermal vent fields. The PACMANUS hydrothermal vent field, located on the Paul ridge, is notable for its distinctly siliceous volcanic host rock (Binns and Scott, 1993; Zeng et al., 2012a). The DESMOS caldera hydrothermal field is located on the southeast ridge in the EMB and hosted by basaltic andesite (Gamo et al., 1997; Park et al., 2010). Abundant CO_2 and excess F in the DESMOS caldera vent fluid indicate magma degassing. The DESMOS caldera basaltic andesite is altered by interaction with hot acidic fluid originating from the mixing of magmatic fluid and seawater (Gena et al., 2001). The Susu Knolls hydrothermal field is in the eastern most part of the EMB and hosted by porphyritic dacitic volcanic rocks, forming three conical peaks informally known as North Su, South Su, and Suzette (Hrischeva et al., 2007). The Solwara 12 hydrothermal field is located 25 km west-northwest of Solwara 1 on the southeastern edge of the DESMOS caldera hydrothermal field. There is extensive sediment cover in the Solwara 12 hydrothermal field, and the mapped hydrothermal chimney field is approximate 200 m across and includes clusters of old hydrothermal sulfide deposit.

2.4.3 North Fiji Basin

The Sonne 99 hydrothermal vent field is located in the North Fiji Basin (NFB) and hosted by volcanic rocks. The volcanic rocks in the NFB include normal MORB (N-MORB) and ocean island basalt (OIB)-related enriched MORB (E-MORB) (Eissen et al., 1994; Nohara et al., 1994; Koschinsky et al., 2002; Kim et al., 2006; Zeng et al., 2017b).

2.5 Shallow-water hydrothermal vent field

The Kueishantao islet is a volcanic center along the southwestern tip of the OT in the west Pacific, located about 10.8 km from Wushi Harbor at Toucheng Town on the Ilan plain. The last major volcanic eruption in

the Kueishantao Islet occurred around 7 ka (Chen et al., 2001). The Kueishantao hydrothermal vent field (KHF) (121°55′E, 24°50′N, approximately 0.5 km²) is situated southeast of the Kueishantao islet (Zeng et al., 2007, 2011) and hosted by andesite, lava flows, and pyroclastics (Chen et al., 2005a, b; Zeng et al., 2013).

3 VOLCANIC ROCKS OF SHVFS

It is well known that the basement rocks of submarine hydrothermal fields significantly impact the chemical characteristics of hydrothermal productions, such as sulfide deposits and vent fluids (Hannington et al., 2005; Zeng, 2011; Humphris and Klein, 2018). The study of volcanic rocks from SHVFs is therefore important for understanding the formation of submarine hydrothermal systems.

3.1 Volcanic rocks of SHVFs in the OT

Most SHVFs in the OT are host by felsic volcanic rocks, and one hydrothermal field is hosted by basalt (Ishibashi et al., 2015).

3.1.1 Origins and evolution of felsic volcanic rocks

The OT is characterized by widespread felsic volcanic rocks with ages of less than 1 Ma (Shinjo and Kato, 2000; Huang et al., 2006; Chen et al., 2018), which is distinct from basalt-dominated intra-oceanic BABs. At present, the origin of the felsic volcanic rocks (rhyolites) in the OT remains uncertain. Type-1 rhyolites in the MOT are produced by re-melting of andesites with residue amphiboles, whereas type-2 rhyolites in the MOT are derived from the re-melting of andesites without residual amphiboles (Zhang et al., 2018a, 2020). The crustal rocks or melts with compositions analogous to those of the andesites from Kueishantao or the upper crustal rocks of southwest Japan might have contaminated the rhyolitic magma in the MOT, suggesting that the OT crust probably contain isotopically enriched crustal materials (Zhang et al., 2020). Nevertheless, both the fractional crystallization of basaltic magma and partial melting of andesites cannot generate melts with a SiO_2 content of 62–68 wt.%, which might shed light on the origin of the compositional gap for bimodal magmatism in the MOT (Zhang et al., 2018a). In contrast, magma mixing plays an important role in controlling the origins of silicic magmas in the southwest OT (Chen et al., 2018, 2019), and the parent magma experienced a multilayer magma chamber systems before eruption (Guo et al., 2018).

3.1.2 Origins and evolution of mafic volcanic rocks

The OT mafic magmatism has been influenced by subduction components (Guo et al., 2017; Shu et al., 2017; Zhang et al., 2018d), which results in the different geochemical imprint of young basaltic rocks. For example, the magma sources of the SOT basalts were principally influenced by subducted fluids and sediments. The magma sources of the MOT basalts were impacted by subducted fluids from both altered oceanic crust and sediment. The geochemical characteristics of the SOT and MOT basalts are variable owing to different Wadati-Benioff depths and tectonic formation environments (Guo et al., 2017). Sediment fluxes account for the Tl isotopic variations in the OT volcanic rocks and require sediments subducted in the range of <1%, 0.1%–1%, and 0.3%–2% from the depleted mantle source to account for the Tl of volcanic rocks from the northern, central, and southern portions of the Ryukyu arc and OT. Bulk sediment mixing is required for the generation of the volcanic rocks from the Ryukyu arc and OT (Shu et al., 2017).

3.2 Volcanic rocks of the SHVFs in the Mid-Ocean Ridge

3.2.1 Geochemical and isotopic analyses of MORBs from EPR 1°S–2°S

MORBs from EPR between 1°S and 2°S show a wide range of trace element and isotopic compositions. One depleted magma source and two enriched magma sources were proposed to contribute to the formation of MORBs from EPR 1°S–2°S. However, basalt samples 02 and 10 from the EPR between 1°S and 2°S were derived from a mixture of enriched and depleted magma sources, whereas basalt sample 07 originated from a depleted magma source that was not influenced by magma mixing (Zhang et al., 2018c).

3.2.2 Silicon and oxygen isotopes in basalts from the EPR

Silicon and oxygen isotopes are two important components in volcanic rocks that are used to trace diagenetic processes, study isotope fractionation, and identify the isotopic characteristics in MORBs from the EPR (Wang et al., 2013a). We found that $\delta^{30}Si$ and $\delta^{18}O$ correlate positively with SiO_2 content, which indicates that the SiO_2 content of MORBs affected the Si and O isotopic fractionation (Wang et al., 2013a).

3.2.3 Geochemical characteristics of abyssal peridotites from the SWIR

In the serpentinite-hosted SHVFs of slow-spreading

Table 1 Physical characteristics and chemical compositions of seafloor hydrothermal vent fluids in different geological environments

Vent fluids	Back-arc basins	Mid-ocean ridges	Volcanic arcs	Seawater
Temperature (°C)	88–334	66–403	39–311	2
pH (25°C, 1 atm)	2.0–5.0	2.6–10.6	1.52–5.2	7.8
Cu (μmol/kg)	<0.01–36	0.3–140	–	<0.003
Zn (μmol/kg)	8–3 000	0.7–900	–	<0.01
Mn (μmol/kg)	12–7 100	0.10–4 480	48–587	<0.001
Fe (μmol/kg)	3–2 500	10–24 100	6–435	<0.001
Pb (nmol/kg)	4–7 000	0–1 085	–	<0.01
W (nmol/kg)	0.76–127	0.06–0.20	0.07–14.3	0.07
Mo (nmol/kg)	6.9–119	2.3–3.9	3.9–135	102
Cd (nmol/kg)	700–1 500	0–910	–	0.7
As (nmol/kg)	84–18 500	<11–1 074	10 944–12 746	23
H_2S (mmol/kg)	1.8–12.4	0.06–35	0.002–1.6	0
CO_2 (mmol/kg)	6–200	3.4–285	39–262	2.3
CH_4 (μmol/kg)	30–7 600	10–3 600	20–140	0
H_2 (μmol/kg)	10–50	40–18 000	25	0

Vent fluid data are from Fouquet et al. (1991), Von Damm (1995), Douville et al. (1999), Pichler and Veizer (1999), Metz and Trefry (2000), Charlou et al. (2002), Glasby and Notsu (2003), Kishida et al. (2004), Hannington et al. (2005), Chen et al. (2005a, b), Rouxel et al. (2008), and Seyfried et al. (2015). –: no data.

MORs, abyssal peridotites contain relics of mantle minerals, which contain primary information about melting and melt extraction processes beneath MORs. In our previous studies, abyssal peridotites from the SWIR near 65°E were comprised mainly of lizardite, chlorite, carbonate, and magnetite with minor amounts of talc, pyroxene phenocrysts, and sparse olivines. Olivine grains in abyssal peridotites from the SWIR near 65°E display exsolution lamellae, indicating the occurrence of talc reduction or decompression during seawater-rock interaction. The abyssal peridotites in the SWIR near 65°E were derived from a depleted mantle magma source that underwent partial melting. Additionally, elemental anomalies (e.g., Rb, Ba, U, Pb, Sr, and Li) and the Ce/Pb ratio imply that these abyssal peridotites in the SWIR near 65°E have been strongly altered by seawater (Zeng et al., 2012b).

4 HYDROTHERMAL PRODUCTS OF SHVFS

4.1 Vent fluids

The vent fluid of SHVFs shows obvious differences in its physical and chemical characteristics (Table 1; Zeng, 2011). The fluids are generally more acidic (although there are also more alkaline hydrothermal fluids, such as the Atlantic Lost City hydrothermal vent field, with a vent fluid pH of 9.8; Hannington et al., 2005) at relatively high temperature (especially hydrothermal vent fluids from black chimneys) with diverse chemical composition, and are clearly affected by subseafloor geological processes and magmatism. However, according to the ejected state of the fluid, it can be divided into focused fluid and diffuse fluid. Compared with magma fluid, the temperature and pressure of hydrothermal fluid is substantially lower and its chemical composition is affected by seawater. The temperature range of vent fluid is large, ranging between 3 and 464°C (Von Damm, 1995). According to the temperature, seafloor hydrothermal vent fluids can be divided into three types: high temperature (>300°C), medium temperature (100–300°C), and low temperature (<100°C). The range of pH value (measured at 25°C) of the vent fluid is also large (1.52–10.6). Compared with seawater, the chemical composition of the end-member fluid has high concentrations of H_2S, Fe, and Mn (Table 1). Furthermore, there are gas components in the vent fluid (CO_2, H_2, H_2S, and CH_4 in bubbles) in shallow-water SHVF, and the CH_4 and H_2 contents in the vent fluid of the black chimney are quite high (CH_4: 25–100 μmol/kg, H_2: 50–1 000 μmol/kg) compared with those of the shallow water hydrothermal vent fluid (CH_4: 0.007–0.200 μmol/kg, H_2: 0.001–0.220 μmol/kg) (Tarasov et al., 2005). This suggests that seafloor hydrothermal activity, cold-seep and gas hydrate may have same methane source and exhibit different methane sinks. Therefore, we propose a new hypothesis of same source and different sinks of seafloor hydrothermal activity, cold-seep and gas hydrate.

4.2 Hydrothermal plumes

4.2.1 Hydrothermal plumes in the OT

The Kuroshio flows from east of Taiwan, China, northwards along the OT, with a maximum speed of 1 m/s and width of 100 km (Liang et al., 2003), which can notably impact the seawater characteristics in the northwestern Pacific. However, the effects of the Kuroshio on the hydrothermal plumes in the OT remain unclear. The results from our previous studies demonstrated that the input of the Kuroshio influences the chemical and physical properties of the hydrothermal plume in the OT, with influence decreasing from the SOT to the MOT (Zeng et al., 2018a).

In the SHVFs of the OT, major elements exhibit

linear correlations in hydrothermal plumes (e.g., B^{3+} and Sr^{2+}), and the anomalous layers show similar element concentrations (Mg^{2+}, SO_4^{2-}) and element ratios (Mg^{2+}/Ca^{2+}, SO_4^{2-}/Mn^{2+}) to those of the OT vent fluids but lower than those of other layers in the hydrothermal plumes. This reveals that the discharge of vent fluid with high concentrations of K^+, Ca^{2+}, and B^{3+} and low concentrations of Mg^{2+} and SO_4^{2-} results in chemical variations of the OT hydrothermal plumes (Zeng et al., 2018a).

The Sr^{2+}/Ca^{2+} and Ca^{2+}/Cl^- ratios in hydrothermal plumes are similar to those of average seawater, suggesting that the chemical properties of local seawater can be inferred from the Sr^{2+}/Ca^{2+} and Ca^{2+}/Cl^- of hydrothermal plumes (Zeng et al., 2018a). Calculated salinity values of hydrothermal vent water and hydrothermal plume water are consistent with measured salinity values (34.3–34.4) of hydrothermal plumes in the MOT and SOT (Fig.1). However, the flux of hydrothermal B^{3+}, Mn^{2+}, Ca^{2+}, and K^+ to seawater in the OT are approximately 0.293–34.7, 1.30–76.4, 1.04–326, and $(2.62–873)\times10^6$ kg/a, respectively, and the heat flux is approximately $(0.159–1\ 973)\times10^5$ W, which implies that approximately 0.000 6% of ocean heat is supplied from seafloor hydrothermal plumes (Zeng et al., 2018a).

4.2.2 Hydrothermal plumes in the EMB

Hydrothermal plumes are potential tools for locating, characterizing, and quantifying seafloor hydrothermal fluid discharge. A neutrally buoyant hydrothermal plume can extend many kilometers (Charlou et al., 1991). Our previous results showed strong positive correlations of arsenic (As) and antimony (Sb) with Mn ($R^2>0.8$) in the hydrothermal plumes of the EMB, and the As/Mn-Mn and Sb/Mn-Mn relationships are exponential without substantial deviation (Fig.2). This demonstrates that As and Sb in EMB hydrothermal plumes can be used to identify the hydrothermal plume as a source and trace the hydrothermal plume spreading movement. However, Cl is depleted relative to ambient seawater in the anomaly layers of hydrothermal plumes at Station 18G and 18K whereas Mn, As, and Sb are slightly enriched, which reflects the contribution of Mn-As-Sb-rich and Cl-poor vent fluid. The hydrothermal plume at Station 18B is slightly enriched in Cl and significantly enriched in Mn, As, and Sb, reflecting the contribution of a Mn-As-Sb-Cl-rich vent fluid (Zeng et al., 2018b).
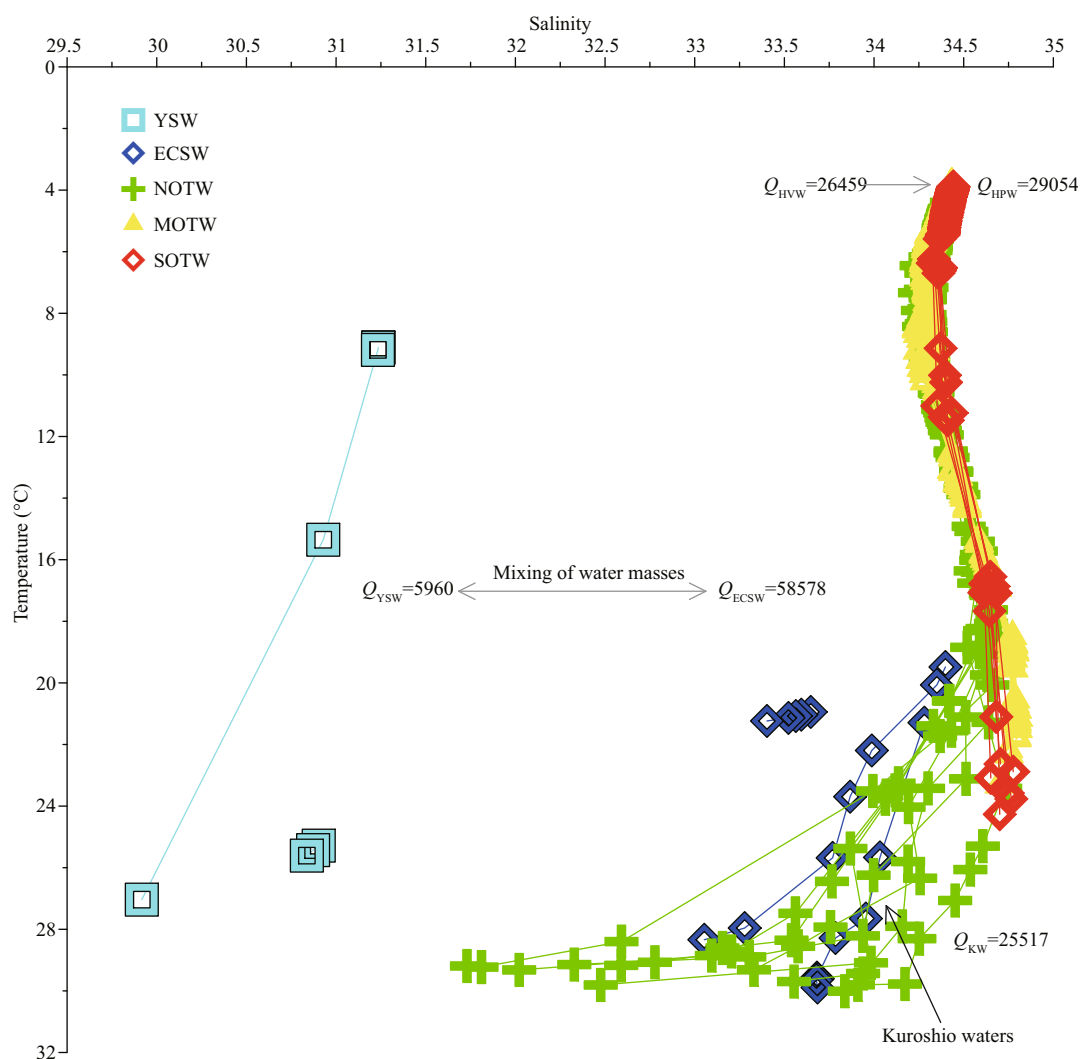
4.3 Hydrothermal sulfides

4.3.1 Re-Os abundance and isotopic compositions of hydrothermal sulfides

Little is presently known about the Re-Os isotopic composition of hydrothermal sulfides from SHVFs in MORs and BABs owing to their low concentrations in seafloor hydrothermal sulfides and the difficulty in obtaining pure hydrothermal sulfide samples. We found a limited range of most $^{187}Os/^{188}Os$ radios (1.004–1.209) of hydrothermal sulfides in the SHVFs from MORs and BABs. This indicates that Os in hydrothermal sulfide is mainly from seawater and therefore clarified as a seawater-derived component. The initial $^{187}Os/^{188}Os$ isotopic compositions of ancient seafloor hydrothermal sulfides might thus be a useful proxy for understanding the Os components of ancient seawater because ancient seafloor hydrothermal sulfides were also produced by the mixing of seawater and vent fluid (Zeng et al., 2014a). The Re and Os of vent fluids in SHVFs are more likely to be incorporated into Fe- and Fe-Cu sulfide mineral facies and Os enriched under low-temperature (<200°C) hydrothermal conditions. Moreover, $^{187}Os/^{188}Os$ values of LHF sulfide samples are lower than those of ambient seawater, which might be affected by seawater Os and MORBs and/or ultramafic rocks (Fig.3). The Re-Os data of seafloor hydrothermal sulfides have also been used to estimate that SHVFs contain roughly 0.6 to 44 t of Re, and 1–48 kg of Os, and the Os flux of hydrothermal fluids to vents is about 11 kg/a in SHVFs worldwide (Zeng et al., 2014a).
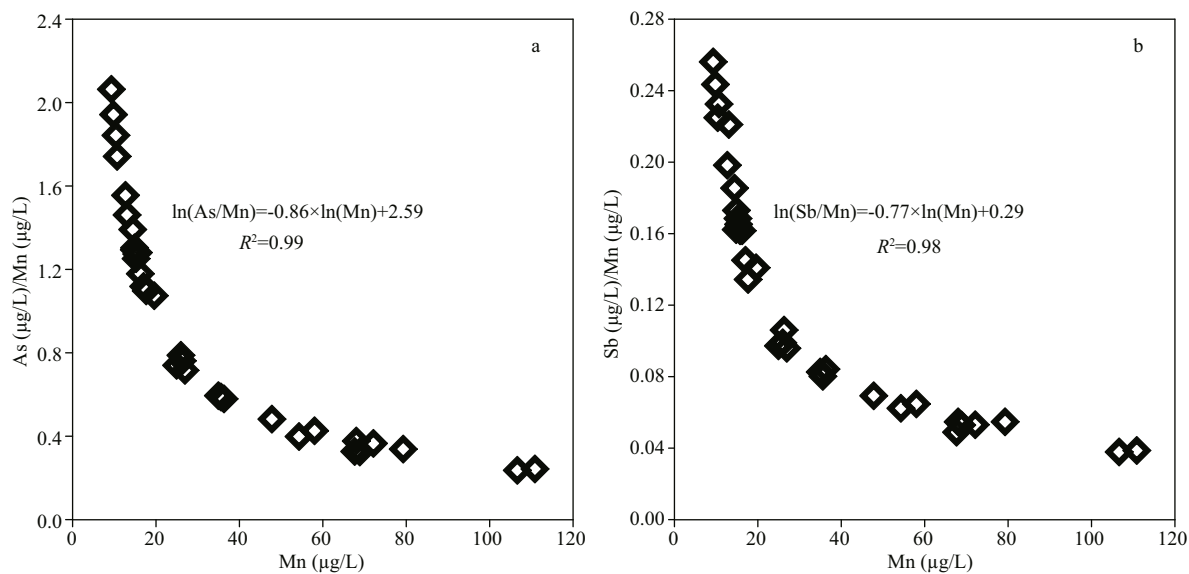
4.3.2 Noble gases in hydrothermal sulfides

Vent fluid temporal variability in SHVFs can be reconstructed by studying noble gases in seafloor hydrothermal sulfides, which can also extend our knowledge of the historical helium (He)/heat ratio of the seafloor hydrothermal geological record (e.g., Zeng et al., 2001, 2004). Noble gas composition data for fluid inclusions in seafloor hydrothermal sulfides, sulfates, and opal samples from seafloor hydrothermal sulfides in MORs and BABs settings remain scarce. The results of our previous study showed that the He isotopic ratios and concentrations in hydrothermal sulfide samples are variable ($^3He/^4He$=0.6–10.4 Ra; ^4He=$(0.12–22)\times10^{-8}$ cm^3 STP/g). Low-temperature vent fluids lose their mantle He in SHVFs during cooling, which leads to higher He concentrations in
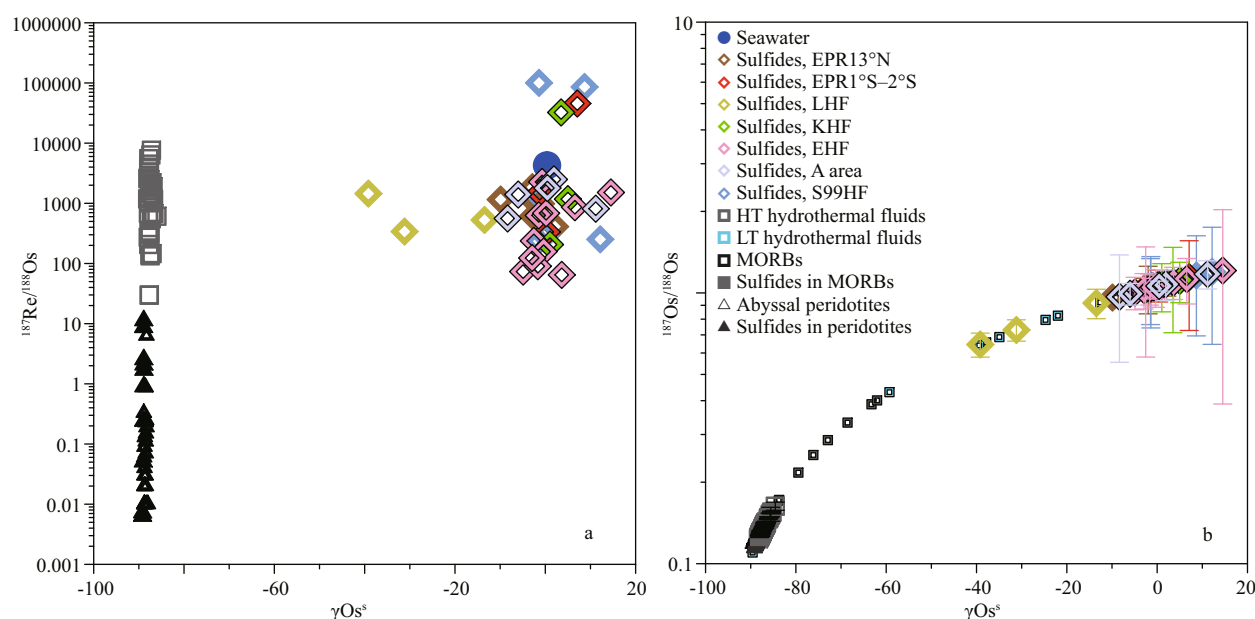
Fig.1 Salinity and temperature in seawater columns and annual water budget in the OT, East China Sea, and Yellow Sea

YSW: Yellow Sea water; ECSW: East China Sea water; NOTW: NOT water; MOTW: MOT water; SOTW: SOT water; HVW: hydrothermal vent water; HPW: hydrothermal plume water; KW: Kuroshio water. Q_{KW}: $Q_{SW}+Q_{TW}+Q_{IW}$, where Q is the water flux in units of weight (Gtons).

Fig.2 Variations in As/Mn (a) and Sb/Mn (b) ratios with Mn in the EMB plume

Fig.3 γOsˢ versus $^{187}Re/^{188}Os$ (a) and γOsˢ versus $^{187}Os/^{188}Os$ (b)

HT and LT hydrothermal fluid data are from Sharma et al. (2000) and Sharma et al. (2007). Data of MORBs and their hosted sulfides are from Schiano et al. (1997) and Gannoun et al. (2007). Data of abyssal peridotite and their hosted sulfides are from Snow and Reisberg (1995) and Harvey et al. (2006). Seawater data is from Peucker-Ehrenbrink and Ravizza (2000).

most sulfide samples than in opal ($^4He=(0.017–0.028)\times10^{-8}$ cm³ STP/g). The distinct $^3He/^4He$ ratios of hydrothermal sulfides in SHVFs originated from different He sources. Specifically, sulfide samples with high $^3He/^4He$ ratio (>7 Ra) mainly stem from mantle source (MORB or OIB) by magma degassing, whereas the sulfide samples with intermediate (1–7 Ra) and low (~1 Ra) $^3He/^4He$ ratios are derived from the mixing of fluid and seawater and ambient seawater, respectively. The $^3He/^4He$ ratios of sulfides reveal that low-temperature sulfides, sulfates, and opal minerals do not retain the He isotopic compositions of the primary high-temperature vent fluid, whereas high-temperature sulfides do in global SHVFs (Zeng et al., 2015a). However, the concentrations of other noble gases (e.g., Ne, Ar, Kr, Xe), in seafloor hydrothermal sulfides are significantly lower than in sulfate and opal mineral samples in global SHVFs. Barite and opal minerals are characteristic of low-temperature (<200°C) hydrothermal paragenetic associations and the Kr concentrations in our samples show positive correlations with Ne and Ar concentrations (Fig.4). This indicates that heavier noble gases are enriched under low-temperature hydrothermal conditions, which is most easily explained by the dominance of a seawater-derived component in SHVFs (Zeng et al., 2015a). Additionally, global He and heat fluxes to high-temperature fluid vents obtained from He/heat

ratios are about $(0.05–6)\times10^4$ kg/a and $0.1–12\times10^{12}$ W, respectively, implying that high-temperature hydrothermal activity in global SHVFs supplies approximately 0.3% of the ocean heat (Zeng et al., 2015a).

4.3.3 Rare earth element (REE) compositions of hydrothermal sulfides

The study of REEs in seafloor hydrothermal sulfides is the key to evaluating the sources of hydrothermal fluid constituents, mixing processes, hydrothermal fluid evolution, and physicochemical conditions of hydrothermal fluids (Zeng et al., 2009). Limited REE composition data are presently available for seafloor hydrothermal sulfides from various SHVFs in MORs and BABs. Our previous results showed that the majority of REE distribution patterns in the global seafloor sulfides from the MORs and BAB exhibit light REEs (LREEs) enrichment, which is similar to that of fluids in SHVFs. However, the seafloor sulfides in global SHVFs have variable REE concentrations, Eu anomalies, and fractionation between LREEs and heavy REEs (HREEs), which are related to the REE compositions of the sulfide-forming fluids and chemical compositions of the sulfide minerals. Furthermore, REE substitution into seafloor Fe-, Cu-, and Zn-rich sulfides appears to be strongly influenced by crystallographic control (Mills and Elderfield, 1995) and the total REE concentrations
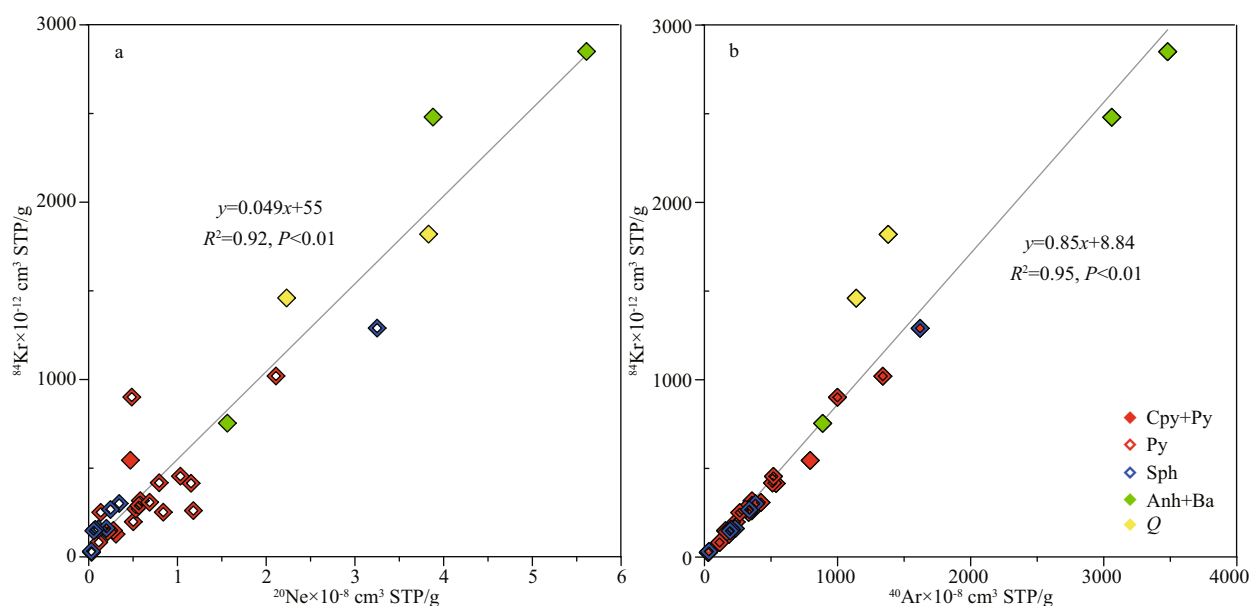
Fig.4 Variations of Ne and Kr concentrations (a), Ar and Kr concentrations (b) in seafloor hydrothermal sulfides, sulfates, and opal mineral aggregate samples

and variation range of seafloor Fe-rich sulfides are all larger than those of Cu- and Zn-rich sulfides, which suggests that REEs of hydrothermal fluids are more easily incorporated into Fe-rich sulfides during seafloor hydrothermal sulfide mineral precipitation in SHVFs (Fig.5).
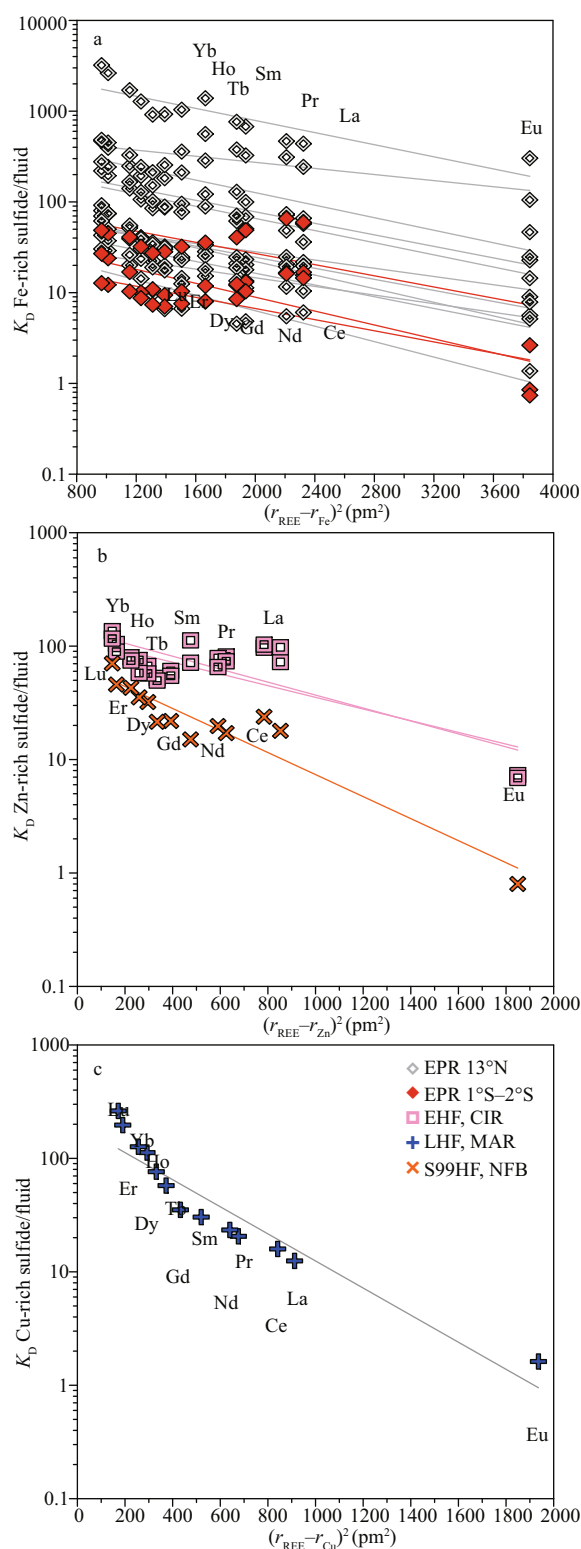
Based on the seafloor sulfide REE data, we estimate that SHVFs hold approximately 280 t of REEs. According to the flux and mean REE concentration (3 ng/g) of vent fluids at MORs, vent fluids in SHVFs alone transport up to 360 t of REEs to the oceans over a two-year period, which is higher than the total quantity of REEs in seafloor sulfides. Excess REEs may be transported away from the SHVFs and become bound in seafloor sulfate deposits, metalliferous sediments, Fe-Mn crusts, and nodules distal to the SHVFs (Zeng et al., 2015b).

4.3.4 S and Pb isotopic compositions of hydrothermal sulfides

Sulfur (S) and lead (Pb) isotopes are powerful tracers for exploring seafloor hydrothermal processes, fluid-rock interaction, magmatic activity, and S and Pb sources in SHVFs (Zeng et al., 2010b). Our previous results indicated that the S isotopic compositions of the seafloor sulfides in SHVFs from MORs and BABs are variable (δ^{34}S from 0.0 to +9.6‰), and S in seafloor sulfides is derived from associated volcanic rocks (e.g., ~0‰ for basalt) and seawater. Compared with the S isotopic compositions
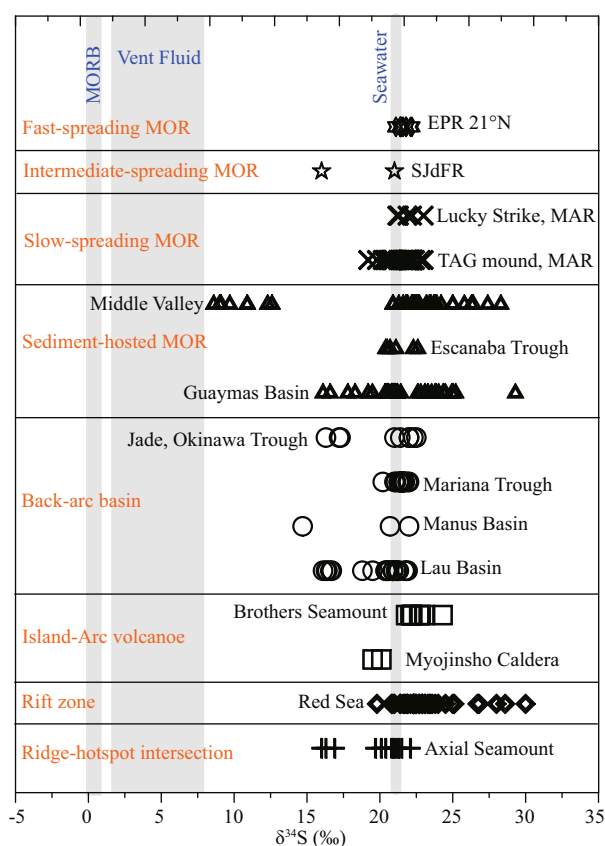
of seafloor hydrothermal sulfates from sediment-hosted MORs, the variation range of S isotopic compositions of hydrothermal sulfates from sediment-starved MORs is also smaller in SHVFs (Fig.6), and S in the sulfate samples is derived mainly from seawater S. However, owing to the lower degree of fluid-rock interaction and fluid-seawater mixing, the δ^{34}S variation range of seafloor sulfide minerals from super-fast and fast spreading MORs is limited in contrast to the wider δ^{34}S range of sulfides from super-slow and slow spreading MORs.

In contrast to a mixed origin for the source of S, the majority of the Pb isotopic compositions (^{206}Pb/^{204}Pb=17.541±0.004 to 19.268±0.001, ^{207}Pb/^{204}Pb=15.451±0.001 to 15.684±0.001, ^{208}Pb/^{204}Pb=37.557±0.008 to 38.988±0.002) from seafloor sulfides in SHVFs from MORs and BABs are similar to those of local volcanic rocks (e.g., basalt), which reveals that Pb in sulfide from sediment-free MORs and mature BABs is mainly leached from host volcanic rocks. However, Pb isotope ratios of hydrothermal sulfides on sediment-hosted MORs (e.g., Middle Valley) show a larger range than those of hydrothermal sulfides from sediment-starved MORs (e.g., EPR 1°S–2°S) (Fig.7). Additionally, we demonstrate that variable S and Pb isotopic compositions of seafloor hydrothermal sulfides exhibit a relationship with the S and Pb sources, fluid-rock and/or sediment interaction, and fluid-seawater mixing in SHVFs (Zeng et al., 2017b).

Fig.5 K_D versus $(r_{REE}−r_{element})^2$ in Fe-rich sulfides (a), Zn-rich sulfides (b), and Cu-rich sulfide (c)

K_D: the distribution coefficient of each REE between the sulfide and vent fluid, $K_D=C_s/C_f$, where C_s is REE concentration in sulfide; C_f: the REE concentrations in vent fluid, and r_{REE} and $r_{element}$ are the ionic radii of the REE and Fe, Zn, and Cu cation that undergo substitution, respectively (Mills and Elderfield, 1995). Solid lines indicate the correlation between K_D and $r_{REE}−r_{element}$ in sulfides.
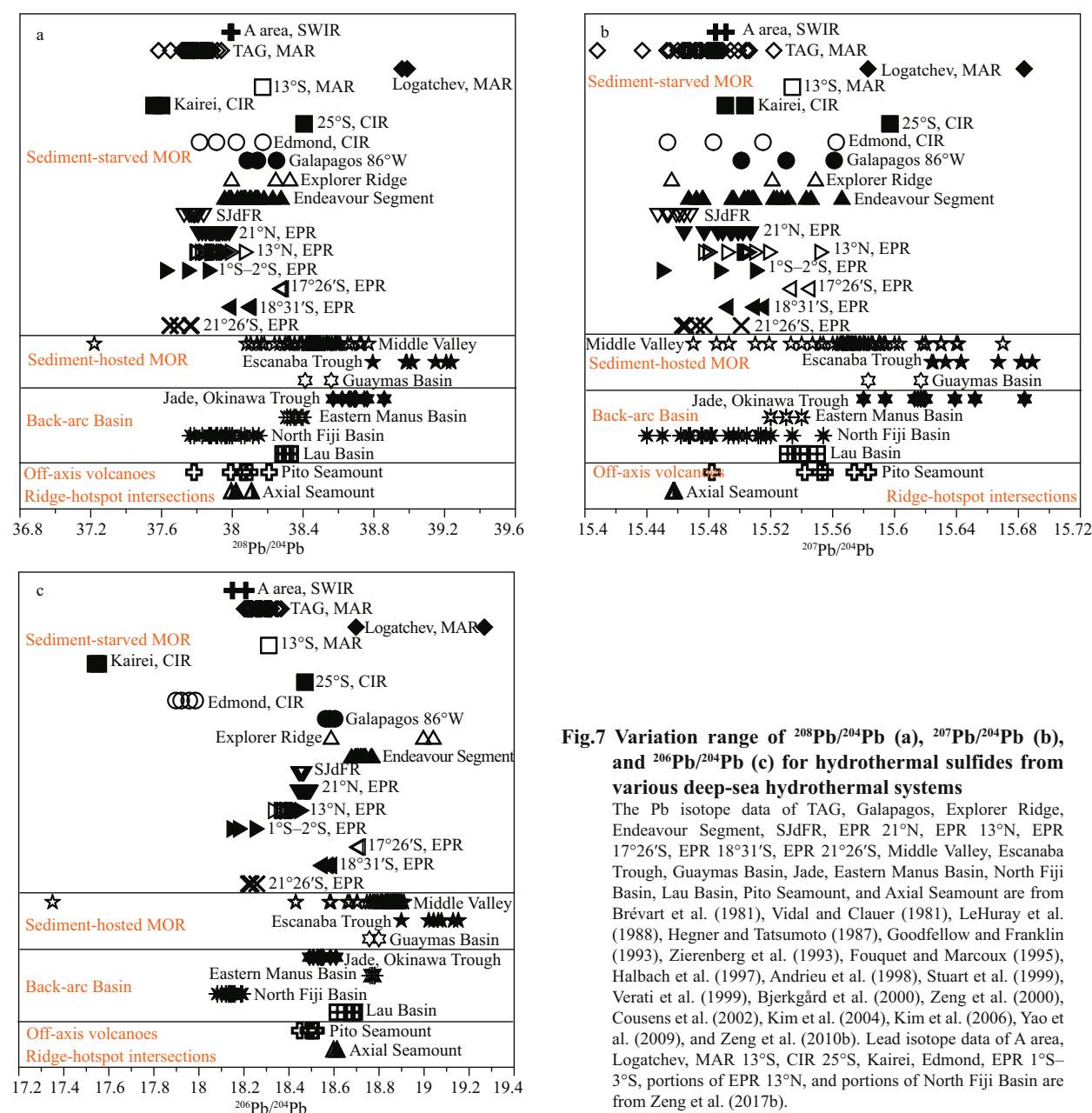

Fig.6 Sulfur isotope values of sulfates from various SHSs

MORB data are from Sakai et al. (1984). Seawater data are from Rees et al. (1978). Vent fluid data are from Shanks III and Seyfried (1987), Woodruff and Shanks III (1988), Halbach et al. (1989), and Kusakabe et al. (1990).

4.3.5 Mineralogical, and chemical characteristics of sulfides from the EPR

Studies of the structure, mineral, and chemical compositions of seafloor hydrothermal sulfides can help us understand the hydrothermal fluid evolution and elucidate the interaction between subseafloor hydrothermal fluid and rock, as well as the material contributions of seawater (Zeng et al., 2009). However, studies on REEs and rare and dispersive elements of seafloor hydrothermal sulfides from the EPR near 13°N are scarce, and variations in seafloor hydrothermal sulfides under the influence of seawater remain poorly constrained (Zeng et al., 2010b). Seafloor hydrothermal sulfides from the EPR near 13°N include Zn-enriched sulfides, which are composed mainly of sphalerite, chalcopyrite, and pyrite. Fe contents and $\delta^{34}S$ values increase progressively from high- to low-temperature sulfide mineral assemblages, whereas Zn contents and Pb isotopic ratios progressively decrease. The phenomenon suggests that the effects of seawater on element distributions (Fe, Zn) and isotopic

Fig.7 Variation range of $^{208}Pb/^{204}Pb$ (a), $^{207}Pb/^{204}Pb$ (b), and $^{206}Pb/^{204}Pb$ (c) for hydrothermal sulfides from various deep-sea hydrothermal systems

The Pb isotope data of TAG, Galapagos, Explorer Ridge, Endeavour Segment, SJdFR, EPR 21°N, EPR 13°N, EPR 17°26′S, EPR 18°31′S, EPR 21°26′S, Middle Valley, Escanaba Trough, Guaymas Basin, Jade, Eastern Manus Basin, North Fiji Basin, Lau Basin, Pito Seamount, and Axial Seamount are from Brévart et al. (1981), Vidal and Clauer (1981), LeHuray et al. (1988), Hegner and Tatsumoto (1987), Goodfellow and Franklin (1993), Zierenberg et al. (1993), Fouquet and Marcoux (1995), Halbach et al. (1997), Andrieu et al. (1998), Stuart et al. (1999), Verati et al. (1999), Bjerkgård et al. (2000), Zeng et al. (2000), Cousens et al. (2002), Kim et al. (2004), Kim et al. (2006), Yao et al. (2009), and Zeng et al. (2010b). Lead isotope data of A area, Logatchev, MAR 13°S, CIR 25°S, Kairei, Edmond, EPR 1°S–3°S, portions of EPR 13°N, and portions of North Fiji Basin are from Zeng et al. (2017b).

compositions (S, Pb) are enhanced during seafloor sulfide formation. Furthermore, seafloor weathering accounts for the enrichment of V, Mn, and REEs in the sulfide-oxidation layer, which results in identical REE patterns for the oxidation layer and seawater. Weathering also distinctly affects the correlations between element ratios of seafloor sulfides (Zeng et al., 2010b).

4.3.6 Geochemical and U-series isotopic characteristics of sulfides in the OT

The characteristics of rare and dispersive elements of seafloor hydrothermal sulfides from the Jade hydrothermal field in the OT and REEs composition of seafloor hydrothermal sulfides bearing sulfate remain unclear and their chronological ages are poorly constrained. Our previous results demonstrated that LREEs are relatively enriched in the sulfate-bearing hydrothermal sulfide samples from the Jade hydrothermal field in the OT, and all the fresh seafloor hydrothermal sulfide samples belong to Zn-rich hydrothermal sulfides. However, the Au and Ag contents in the hydrothermal sulfides from the Jade hydrothermal field in the OT are related to Fe-sulfide, because low temperature promotes Au and Ag enrichment in seafloor hydrothermal sulfides. Based

on the ^{210}Pb/Pb ratios of the hydrothermal sulfide samples, their U isotopic composition, and ^{232}Th and ^{230}Th concentrations are at base level and the formation age of the seafloor sulfide from the Jade field in the OT is between 200 and 2000 years (Zeng et al., 2009).

4.4 Hydrothermal alteration

4.4.1 Hydrothermal altered pillow basalts from the EPR

Seafloor hydrothermal fluid-basalt interaction at MORs is known to play an important role in chemical exchange between seawater and oceanic crust. However, previous studies of basalt alteration mainly focused on subseafloor samples, whereas the alteration of basalts exposed on the seafloor is less known. We found several types of hydrothermal alteration in pillow basalts from the EPR near 13°N. Variations of Al, Si, and Fe concentrations at the edges of plagioclase micro-phenocrysts in the hydrothermal altered basalt are 17.59%, 10.69%, and 109%, respectively. Analogously, variations of Al, Si, and Fe concentrations at the edges of basaltic glass are 16.30%, 9.79%, and 37.83%, respectively, owing to interaction between fluids and pillow basalt (Zeng et al., 2014b).

4.4.2 Pumice affected by hydrothermal fluids

Hydrothermally altered pumice can record information about the variation or evolution of seafloor hydrothermal systems. The results in our previous studies showed that fluids have at least two-stage effects on T3-3 pumice samples near the Iheya North field in the MOT. In the first stage, amorphous silica precipitated from fluid into the vesicles of the pumice owing to conductive cooling and fluid-seawater mixing. In the second stage, the pumice suffered low-temperature alteration while precipitated amorphous silica re-dissolved, leading to Si and Fe deficits and Mg, Zn, Pb, and Cu enhancements in the altered pumice. The change from silica precipitation to re-dissolution in the altered pumice might imply increasing temperature and/or decreasing silica concentrations in the fluids, suggesting a change of hydrothermal environment. Furthermore, ferruginous filamentous silica, which might be related to Fe-oxidizing bacteria, also formed in the hydrothermal altered pumice (Zhang et al., 2018b).

4.5 Hydrothermal Fe-Si-Mn-oxyhydroxides

4.5.1 Hydrothermal Fe-Si-Mn-oxyhydroxides in the EPR

Fe-oxyhydroxides have been discovered at many

SHVFs, which occur either as chimneys, mounds, interstitial precipitates filling cracks between lava flows, or as irregularly shaped edifices. In our published studies, amorphous Fe-oxyhydroxide samples from the EPR near 13°N with a few sphalerite microlites were formed by secondary oxidation in a low temperature, oxygenated hydrothermal environment (Zeng et al., 2008). However, the Fe-oxyhydroxide samples have similar trace (As, Co, Ni, Cu, Zn) and major element (Fe, Ca, Al, Mg) concentrations to those of sulfides, suggesting that the Fe-oxyhydroxide represents a secondary oxidation product of seafloor sulfides. Furthermore, Fe-oxyhydroxide samples have lower ΣREE contents with a notably negative Ce anomaly (0.12–0.28), and their chondrite-normalized REE patterns are similar to those of seawater, which are distinct from the REE compositions of hydrothermal plume particles and vent fluids. These results suggest that the REEs of the Fe-oxyhydroxide are derived mainly from seawater and the Fe-oxyhydroxides might be a sink of REEs from seawater in the SHVFs. Furthermore, the quick settling of hydrothermal plume particles resulted in lower REE contents and higher Mn contents in these Fe-oxyhydroxides, which are captured in part by V and P from the seawater through adsorption (Zeng et al., 2008). Recognizing the mineralogy, geochemistry, and generation of Fe-Si-Mn-oxyhydroxides in seafloor hydrothermal geological environments is an important component for understanding ancient volcanogenic massive sulfide deposits (Zeng et al., 2012c).

Altered seafloor basalt samples from the EPR near 13°N are analyzed (Zeng et al., 2014b) to obtain a clearer understanding of the role of hydrothermal and hydrogenetic processes in the formation of Fe-Si-Mn-oxyhydroxide encrustations on MORBs. The results show that these encrustations are mainly composed of 1–2 mm thick amorphous Fe-Si-Mn-oxyhydroxides that are characterized by laminated, spherical, porous aggregates with several bio-detritus, anhydrite, nontronite, and feldspar particles. However, the Fe-Si-Mn-oxyhydroxide encrustations contain anhydrite particles and nontronite crystals, which indicate that these encrustations may have formed under relatively low- to high-temperature hydrothermal conditions. Their growth rate suggests that they are unlikely to have resulted from hydrogenic deposition alone but have a hydrothermal and hydrogenic origin, and formed during several stages of seafloor hydrothermal activity. During the initial formation stage of the Fe-

Si-Mn-oxyhydroxide encrustations, dense and Mn-poor Fe-Si-oxyhydroxides were deposited from a relatively reducing fluid and loose Fe-Si-Mn-oxyhydroxides are subsequently deposited on them. Furthermore, Si-oxide is inhibited and Mn-oxide will precipitate with Fe-oxyhydroxides owing to the increasing oxidation state of the seafloor fluid in the SHVFs (Zeng et al., 2014b).

4.5.2 Hydrothermal Fe-Si-Mn oxyhydroxides in the EMB

The geochemistry and temperature gradients produced by the mixing of oxidized seawater and reduced fluids deliver an appropriate environment and energy sources (CH_4, H_2S, CO_2, Fe^{2+}, and Mn^{2+}) for microbial growth in the SHVFs, which further affect the formation and microstructure of HPs. Previous studies have proposed that neutrophilic Fe-oxidizing bacteria play a key role in the generation of Fe-Si oxides in SHVFs (Emerson and Moyer, 2002; Edwards et al., 2011). However, the competitive relationship between abiotic and biotic oxidation reactions and abiotic and biotic kinetic mechanisms in Fe oxidation remain unclear. Our previous results show that Fe-Si oxide samples from the PACMANUS hydrothermal vent field in the EMB had abundant rod-like or twisted filamentous and granular structures composed mainly of Fe and Si. However, the amount of Fe oxides around the hydrothermal vent was larger than the amount determined by strict abiotic kinetic calculation in the EMB (Yang et al., 2015).

In the PACMANUS hydrothermal vent field, the Fe-Si-Mn-oxyhydroxides constituted by Fe- and Mn-oxyhydroxides with opal-A and nontronite, have extremely low contents of trace elements (exclusive of Ba, Mo, V, and U) and REEs, and show REE distribution patterns with positive Eu anomalies and slight LREEs enrichments. The differences in REE distribution patterns between the Fe-oxyhydroxide fraction and Mn-oxyhydroxide fraction originate from diagenetic processes in the EMB. Furthermore, there are various filamentous micro-textures that are similar to unique microbial populations, implying that microbially-mediated mineralization occurred during the formation of Fe-Si-Mn-oxyhydroxides (Zeng et al., 2012a). We proposed an original model for the formation of Fe-Si-Mn-oxyhydroxides in the PACMANUS hydrothermal vent field (Zeng et al., 2012a).

Furthermore, there are micro-textures in the Fe-Si-Mn-oxyhydroxide samples from the PACMANUS hydrothermal vent field in the EMB that resemble

fossil microbes such as filamentous silica and hollow pipes. Our previous results showed that flakes of nontronite crystals precipitated from low-temperature fluids and microbes may have affected their formation. The nontronite crystals either developed a honeycomb texture or dispersed on the surface of the hollow pipes. Moreover, we found that Si-Fe-Mn-oxyhydroxides from the PACMANUS hydrothermal vent field in the EMB have two types of nuclei: Si-Mn nuclei and Si nuclei, both of which are encircled by similar Si-Fe outer layers in the rod-shaped oxyhydroxide and spheroidal oxyhydroxide, respectively. The formation of Si-Mn nucleus is closely related to microbes, whereas Si nucleus is of inorganic origin (Zeng et al., 2012c).

4.6 Hydrothermal metalliferous sediments

4.6.1 Smectite minerals from the EPR near 13°N

The formation mechanism of authigenic smectite and its material source in metalliferous sediments can reflect the interactions between seafloor hydrothermal activity and non-hydrothermal mineral phases. However, authigenic smectite in global marine sediments has different origins, and the origin of smectite minerals in the SHVFs from EPR remains unclear. We reported new data on smectite minerals from the EPR near 13°N. The reaction of Fe-oxyhydroxide with silica, as well as seawater in metalliferous sediments, is responsible for the generation of the smectite minerals. The Si in the smectite minerals may originate from siliceous microfossils (diatoms or radiolarians), detrital mineral phases, or vent fluids. In contrast to authigenic smectites, these smectites have higher $\delta^{30}Si$ owing to selective absorption of light Si isotopes onto Fe-oxyhydroxides during the formation of hydrothermal smectite. The large ionic radii of REEs likely prevent substitution in either the tetrahedral or octahedral lattice sites in the structure of hydrothermal smectite. Thus, REEs are lost and scavenged by Fe-oxyhydroxides during the formation of hydrothermal smectite, which reduces the value of metalliferous sediments as a latent resource for REEs in the SHVFs (Rong et al., 2018).

4.6.2 Major and trace elements in SMAR sediments

Sulfides, Fe-Mn oxides, and oxyhydroxides precipitated from hydrothermal plumes may scavenge metal elements from seawater and settled into the sediment surrounding hydrothermal vents. Our

previous studies revealed high elemental contents (e.g., Fe, Mn, Cu, Zn, V, and Co) in samples from the metalliferous sediments near SHVFs in the SMAR, whereas other element concentrations (e.g., Sr, Ca, and Ba) in the metalliferous sediment samples displayed reverse trends, and positive correlations between Fe and Zn, Cu, Ni, Co, Pb, and V contents were observed. These results are consistent with the chemical evolution of dispersing hydrothermal plumes from SHVFs (Huang et al., 2017a).

4.7 Organic matter in the hydrothermal vent fields

4.7.1 Hydrocarbons in sediments from the NOT

The discovery of seafloor hydrothermal activity offers a new motivation for understanding the nature of organic matters (OM) in SHVFs (Lein et al., 2003; Simoneit et al., 2004). We measured the abundance and distribution of hydrocarbons in the sediment core from the NOT. The data demonstrate that n-alkanes in this sediment core exhibit a bimodal distribution and an odd-to-even predominance of high molecular weights compared with an even-to-odd predominance in low molecular weight n-alkanes. Moreover, the distribution and composition of hydrocarbons in this sediment core indicate that one or several unobserved SHVFs may exist in the NOT (Huang et al., 2017b).

4.7.2 Abundance and distribution of polyaromatic hydrocarbons in SMAR sediments

Polyaromatic hydrocarbons (PAHs) generally have two to seven or more conjugated aromatic rings and are stable under high-temperature hydrothermal conditions. We measured the abundance and distribution of PAHs from SMAR sediment samples and compared with PAHs values from sediments of different distances from the SHVFs (Huang et al., 2014). The previous results showed that ΣPAHs is higher in sediment samples near the SHVFs and lowest in sediment samples farthest away from the SHVFs, implying a plausible hydrothermal origin for ΣPAHs. Moreover, sample 22V-TVG10 showed a maximum ratio between the parent methylphenanthrene and phenanthrene, which likely reflects the degree of seafloor hydrothermal alteration and indicates that the PAHs of SMAR sediments mainly originated from hydrothermal alteration (Huang et al., 2014).

4.7.3 Organic constituents of hydrothermal barnacles and sediments from the SWIR

Previous studies have investigated the OM of

hydrothermal fluids, sulfides, rocks, and sediments, and the organic components of tubeworms, bivalves, gastropods, shrimp, crabs, and fish from SHVFs. The results showed that high concentrations of aromatic compounds in hydrothermal barnacle and sediment samples from the SHVFs in the SWIR might result from macromolecular hydrothermal alteration. Microorganism, especially those associated with sulfur metabolism in the SHVFs, might be the source of high concentrations of fatty acids detected in the hydrothermal barnacle and sediment samples from the SWIR. Moreover, n-alkanes might originate from the hydrothermal alteration of carboxylic acids and other lipid compounds in the high temperature and pressure hydrothermal environments of SHVFs in the SWIR (Huang et al., 2013).

4.8 Organisms in hydrothermal vent fields

4.8.1 Chemical compositions of mussels and clams

Studies of the chemical characteristics of mussels and clams in SHVFs are important for understanding the concentrations, transport, and biological effects of chemicals in mussels and clams, as well as the mass fluxes and elemental partitioning from seafloor hydrothermal vents into the oceanic biosphere, metal bioaccumulation of seafloor hydrothermal systems, and the sources and sinks of biogeochemical and fluid cycles. This information helps assess the organisms' biosorption capacity for metals, the transmission of elements between animals and fluids and/or rocks, the roles of metals in the metabolism of the hydrothermal animals, and the mechanism of metal toxicity in the SHVFs (Zeng et al., 2017a).

However, the influence of hydrothermal environment on the behavior of vent mussels and clams in the OT remains unclear. We analyzed the concentrations of major elements, trace elements, and REEs, as well as the carbon and oxygen isotope compositions in the tissues and shells of mussels and clams from the Tangyin and Yonaguni Knoll IV fields in the SOT (Zeng et al., 2017a). The data show linear correlations between metal elements in the shells and tissues of the mussels and clams. The Zn, Mo, and Pb contents in clam tissues vary by tissue type, suggesting that not all positive correlations of the elements in the tissues are inherited by the shells in the SHVFs. Moreover, the element ratios (V/As, Ca/Sr, and Fe/Cr) in the mussels and clams are similar to those of the seawater, implying that the element ratios of seawater might be inherited by organisms from seafloor hydrothermal field, which suggests that the

V/As and Fe/Cr ratios of the mussel and clam shells can be used to trace local seawater composition in the SHVFs (Zeng et al., 2017a). However, the mussel and clam tissue samples have high total LREE concentrations, LREE enrichment, and no or only slightly negative Eu anomalies, indicating that the mussels and clams in SHVFs are a sink of LREEs from fluids.

Furthermore, the $\delta^{13}C$ values of the mussel shells are heavier than those of the clam shells, implying that more than one carbon source is required for explaining the $\delta^{13}C$ compositions of the shells. However, the $\delta^{18}O$ values of clam shells are similar to those of the mussel shells and fluid, indicating that the $\delta^{18}O$ values of mussel and clam shell carbonate are affected by fluids (Zeng et al., 2017a).

4.8.2 Chemical compositions of crab and snail

Crabs, clams, mussels, shrimps, tube worms, limpets, cyclopoid copepods, and snails are known to exist in SHVFs. A depiction of the chemical compositions of benthic animals that inhabit SHVFs is crucial for understanding their biomineralization processes, bioaccumulation of metals, chemical transport, and variations under the physic-chemical conditions of the seafloor hydrothermal environment. However, very little is known about the ecology of the Kueishantao hydrothermal field (KHF) and roles of host-rock, fluid and/or plumes in the life history of crabs and snails, as well as the biological and chemical characteristics of snails.

We analyzed the element compositions of crab and snail shells from the KHF (Zeng et al., 2018c) and showed that the element contents (e.g., Mn, Hg, and K) in the male crab shells are higher than those in female crab shells, whereas the reverse is true for the accumulation of boron, which suggests that Mn, Hg, K, and B accumulation in the crab shells in the KHF is sensitive to gender. However, the Li, Mg, and Co concentrations of crab and snail shells range between Kueishantao andesite and vent fluid concentrations, suggesting that Co-enrichment in snail is affected by the Kueishantao andesite (Fig.8). The majority of LREE distribution patterns in the crab and snail shells resemble those of the fluids, with LREEs enrichment, indicating that the LREEs in the crab and snail shells originate from fluids in the KHF (Zeng et al., 2018c).

5 SHALLOW-WATER HYDROTHERMAL ACTIVITY IN THE KHF

The vents in the KHF can be classified into two types: yellow spring and white spring. The temperature of the yellow-spring fluids (78–116°C) is higher than that of the white-spring fluids (30–65°C) (Chen et al., 2005a, b; Zeng et al., 2013), and the temperature variation of the vent fluids is associated with diurnal tides, reaching a maximum 2–4 h after each high tide (i.e., high pressure) (Kuo, 2001; Chen et al., 2005a, b). The yellow-spring fluids are characterized by extremely low pH (≥1.52) and variable chemical compositions (Chen et al., 2005a, b). The white-spring fluids have relatively low CH_4, Fe, and Cu concentrations (Chen et al., 2005a, b; Zeng et al., 2013). Moreover, native sulfur deposits in the KHF are present in a number of different forms: sand, chimneys, and balls (Zeng et al., 2007, 2011).

5.1 Native sulfur chimney

We previously reported sulfur isotopic compositions of 14 native sulfur samples from a chimney in the KHF. The element compositions of the native sulfur samples suggests that the sulfur of the native sulfur chimney in the KHF (H_2S and SO_2) originated by magmatic degassing, REEs and trace elements in the native sulfur chimneys are mostly derived from Kueishantao andesite and partly from seawater, and relatively low temperature (<116°C), oxygenated, and acidic environment are favorable for the formation of native sulfur chimneys in the KHF (Zeng et al., 2007).

5.2 Native sulfur ball

Native sulfur ball samples have high S contents (up to 99.96 wt.%), similar to native sulfur chimney in the KHF (Zeng et al., 2011). The sulfur contents, REE, and trace element compositions of the native sulfur balls and local environment in the KHF indicate that the slower growth of native sulfur balls results in relatively higher REE and trace element concentrations in native sulfur balls than in native sulfur chimneys. We propose a growth model called "glue pudding" for understanding the origin of native sulfur balls in the KHF, which developed by mixing oxygenated seawater with an acidic, low-temperature fluid containing SO_2 and H_2S gases, which were then shaped by tidal and/or bottom currents (Zeng et al., 2011).

5.3 REE in vent fluids

Numerous investigations of REEs geochemistry of hydrothermal vent systems have been reported, which are critical for understanding sub-seafloor hydrothermal processes, whereas few investigations
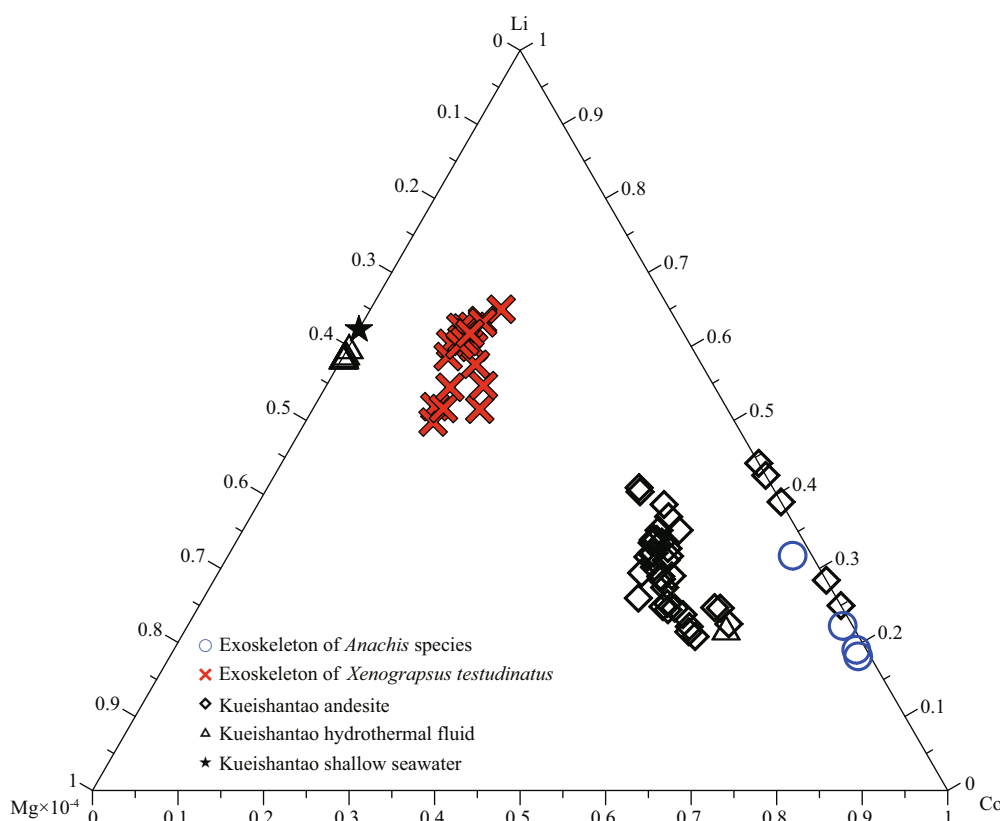
Fig.8 Ternary diagram of Li-Mg-Co in crab and snail shell samples from the KHF in the southwestern tip of the OT

have been conducted on the shallow-water hydrothermal systems of the KHF. Our previous results showed that the total REE concentrations of yellow-spring fluids are notably higher than those of ambient seawater but similar to those of white-spring fluids. The chondrite-normalized REE distribution patterns of the yellow-spring fluids show slight convex-downward curvatures at Eu in contrast to those of the white-spring fluids that show no Eu anomalies, which is attributed to the more oxidizing and low-temperature conditions. Compared with HREEs, LREEs are slightly enriched in KHF fluids and the behavior and patterns of REEs in both yellow- and white-spring fluids are affected by the short water-rock interaction time, exceptionally low pH (2.81 and 2.29), fluid boiling, and precipitation of native sulfur (Wang et al., 2013b).

5.4 Boron in vent fluids and hydrothermal plumes

Seafloor hydrothermal circulation can trigger extensive boron isotopic and chemical exchange, which is controlled by fluid temperatures and sub-seafloor water-rock interactions. Accordingly, the sub-seafloor water/rock ratios are recorded by the boron isotopic compositions in fluids, which provides

an effective method for studying the origin of fluid and hydrothermal processes. However, very little is known about the boron isotope compositions of the shallow-water vents in the KHF, which hinders the understanding of sub-seafloor water-rock interaction and causes bias in the flux quantification of global hydrothermal boron to the oceans (Zeng et al., 2013).

We measured boron concentrations and isotope compositions of seawater, andesite, and fluid and plume samples from the KHF. Fluids and plumes from the yellow and white springs display a regular array of data points, which suggests that the boron in the fluids and plumes is mainly from seawater, rather than from KHF andesite, which further implies that the duration of fluid-andesite interaction is short in the KHF. However, the pH, boron concentrations, and isotopic compositions from fluids to hydrothermal plumes indicate a close relationship with one another, which suggests that the $\delta^{11}B/B$ and pH/B ratios of the hydrothermal plumes have constant values within a small distance (approximately 15 m). This further suggests that the diffusive processes controlling the chemical compositions of hydrothermal plumes in the seawater can be depicted by boron data from the hydrothermal plumes (Zeng et al., 2013). The

subseafloor water/rock ratios are between 1.96 and 3.63 in the KHF, and the hydrothermal flux of boron from the fluids into the oceans is between $6.69×10^4$ and $1.32×10^5$ mol/a (Zeng et al., 2013).

6 CONCLUSION

This paper describes the geological settings and volcanic rocks of SHVFs from MORs and BABs, systematically revealed the material sources and controlling factors of the HPs on global SHVFs, introduces the HP formation model (e.g., hydrothermal sulfide, native sulfur chimney and balls), and indicates that the new means for revealing the formation mechanism of HPs is to expand the research of seafloor hydrothermal vent organisms.

(1) Systematic Re-Os content and isotopic composition of global seafloor hydrothermal sulfides have been studied. Seawater is a significant source of Re and Os in seafloor hydrothermal sulfides and Os is enriched under low-temperature conditions. The $^{187}Os/^{188}Os$ ratios of seafloor hydrothermal sulfides are not controlled by the sulfide mineral facies, and the initial $^{187}Os/^{188}Os$ of ancient sulfides can trace the ancient seawater component. Helium in seafloor hydrothermal sulfides mainly comes from the mantle, whereas Ne, Ar, Kr, and Xe mainly from seawater are enriched in fluid inclusions of low-temperature sulfate and opal. Furthermore, hydrothermal vent fluid provides REEs for global sulfide formation in different tectonic environments, which results in similar LREEs/HREEs ratios between sulfide and hydrothermal fluid. The REEs content and distribution model of seafloor hydrothermal sulfides are restricted by the characteristics of mineral chemical composition, physical and chemical conditions of fluid when sulfide forms, REEs content and distribution model of hydrothermal fluid, mixing degree of hydrothermal fluid and seawater, and interaction between subseafloor fluid and rock. Moreover, the As and Sb of seawater columns can be used to identify the hydrothermal plume as a source and trace hydrothermal plume spreading.

(2) The published results have revealed the material source and formation conditions of native sulfur chimneys and native sulfur balls, established their formation modal, and constrained the relationship with subseafloor geological processes. Compared with deep sea hydrothermal systems, shallow-water hydrothermal systems have their own particularity and complexity. They differ from volcanic hot springs on land and draw attention to the impact of atmospheric precipitation on submarine hydrothermal fluid, impact of tides and typhoons on the growth of HPs such as chimneys, native sulfur balls, and the relationship between earthquakes and hydrothermal activities. The $\delta^{11}B$ values of the vent fluid and hydrothermal plume in the KHF have been determined for the first time, revealing the source and evolution of the fluid. The pH, B content, and $\delta^{11}B$ are significantly related from the vent fluid to the hydrothermal plume. The $\delta^{11}B/B$ and pH/B ratios are stable over short distances (<15 m) from the vent to the hydrothermal plume. The B content and $\delta^{11}B$ value in the hydrothermal plume can be used to describe the diffusion process controlling the chemical composition of the hydrothermal plume in the seawater environment. Furthermore, the hydrothermal fluid and boron in the hydrothermal plume are derived mainly from seawater, with only a small amount from andesite, and the interaction time between the subseafloor fluid and andesite is short. In the first geochemical study of *Anachis* sp. shells from the KHF. We found that element accumulation (K, Mn, Hg, and B) in crab shells is affected by gender via molting, and high metal concentration in snails may be ascribed to long metal accumulation time. LREEs in crab and snail shells originate from hydrothermal fluids.

(3) The formation mechanism of Fe-Si-Mn-oxyhydroxides in the PACMANUS field of the Manus basin in the western Pacific is revealed. Fe-Si-Mn-oxyhydroxides show various filamentary microstructures. Thus, microorganisms play an important role in the formation of Fe-Si-Mn-oxyhydroxides. During the mixing process of hydrothermal fluid and seawater, the mineralization of Fe oxidizing bacteria promoted the precipitation of Si and the existence of bacterial filaments led to the enrichment of U in Fe-Si-Mn-oxyhydroxides, whereas a portion of the Fe-oxyhydroxides were encapsulated with the growth of Mn-oxyhydroxides. Smectite from the EPR near 13°N most likely formed by the reaction of hydrothermal Fe-oxyhydroxide with silica and seawater in metalliferous sediments. Furthermore, volcanism may be the main reason for the observed distribution and composition of hydrocarbons in the sample from the NOT.

(4) A new calculation method of the He/heat ratio is proposed. The contents of Re, Os, and REEs in the global seafloor sulfide deposits are very low (~4 t of Re, ~8 kg of Os, and ~280 t of REEs). The boron flux is between $6.69×10^4$ and $1.32×10^5$ mol/a in the KHF.

We estimated that the global He and heat fluxes are up to 500 kg/a and 1×10^{11} W, respectively, and 0.3% of the ocean heat is provided by high-temperature hydrothermal activity on the seafloor, which provides a new theory and method for overcoming the major problem of hydrothermal geology on the seafloor (i.e., heat and material fluxes).

(5) We propose a multilayer magma chamber system to explain the complex plagioclase crystals in silicic rocks. Our published results indicated that one depleted source and two enriched sources contribute to the formation of MORBs from EPR between 1°S and 2°S. The fractionation of silicon and oxygen isotopes of basalts from the EPR near 13°N is influenced by the SiO_2 content in igneous rocks. The SWIR peridotites originated from a depleted mantle source magma and experienced partial melting.

Combined with the above work, an in-depth view of submarine hydrothermal geology is established, the basic concept of submarine hydrothermal system research is systematically defined, and the types of HPs (e.g., submarine hydrothermal sulfide), are classified in the published book. This provides a theoretical basis for the investigation of submarine hydrothermal geological process, its associated resources, and environmental effects.

7 DATA AVAILABILITY STATEMENT

All data generated and/or analyzed during this study are available from the corresponding author upon reasonable request.

8 ACKNOWLEDGMENT

References

Andrieu A S, Honnorez J J, Lancelot J. 1998. Lead isotope compositions of the TAG mineralization, Mid-Atlantic Ridge, 26°08′N. *Proceeding of the Ocean Drilling Program, Scientific Results*, **158**: 101-109.

Binns R A, Scott S D. 1993. Actively forming polymetallic sulfide deposits associated with felsic volcanic rocks in the eastern Manus back-arc basin, Papua New Guinea. *Economic Geology*, **88**(8): 2 226-2 236.

Bjerkgård T, Cousens B L, Franklin J M. 2000. The Middle Valley sulfide deposits, northern Juan de Fuca Ridge: radiogenic isotope systematics. *Economic Geology*, **95**(7): 1 473-1 488.

Brévart O, Dupré B, Allègre C J. 1981. Metallogenesis at spreading centers: lead isotope systematics for sulfides, manganese-rich crusts, basalts, and sediments from the Cyamex and Alvin areas (East Pacific Rise). *Economic Geology*, **76**(5): 1 205-1 210.

Charlou J L, Bougault H, Appriou P, Jean-Baptiste P, Etoubleau J, Birolleau A. 1991. Water column anomalies associated with hydrothermal activity between 11°40′ and 13°N on the East Pacific Rise: discrepancies between tracers. *Deep Sea Research Part A. Oceanographic Research Papers*, **38**(5): 569-596.

Charlou J L, Donval J P, Fouquet Y, Jean-Baptiste P, Holm N. 2002. Geochemistry of high H_2 and CH_4 vent fluids issuing from ultramafic rocks at the Rainbow hydrothermal field (36º14'N, MAR). *Chemical Geology*, **191**(4): 345-359.

Chen C T A, Wang B J, Huang J F, Lou J, Kuo F W, Tu Y, Tsai H. 2005b. Investigation into extremely acidic hydrothermal fluids off Kueishan Tao, Taiwan, China. *Acta Oceanologica Sinica*, **24**(1): 125-133.

Chen C T A, Zeng Z G, Kuo F W, Yang T F, Wang B J, Tu YY. 2005a. Tide-influenced acidic hydrothermal system offshore NE Taiwan. *Chemical Geology*, **224**(1-3): 69-81.

Chen Y G, Wu W S, Chen C H, Liu T K. 2001. A date for volcanic eruption inferred from a siltstone xenolith. *Quaternary Science Reviews*, **20**(5-9): 869-873.

Chen Z X, Zeng Z G, Wang X Y, Yin X B, Chen S, Guo K, Lai Z Q, Zhang Y X, Ma Y, Qi H Y, Wu L. 2018. U-Th/He dating and chemical compositions of apatite in the dacite from the southwestern Okinawa Trough: implications for petrogenesis. *Journal of Asian Earth Sciences*, **161**: 1-13.

Chen Z X, Zeng Z G, Yin X B, Wang X Y, Zhang Y Y, Chen S, Shu Y C, Guo K, Li X H. 2019. Petrogenesis of highly fractionated rhyolites in the southwestern Okinawa Trough: constraints from whole-rock geochemistry data and Sr-Nd-Pb-O isotopes. *Geological Journal*, **54**(1): 316-332.

Cousens B L, Blenkinsop J, Franklin J M. 2002. Lead isotope systematics of sulfide minerals in the Middle Valley hydrothermal system, northern Juan de Fuca Ridge. *Geochemistry, Geophysics, Geosystems*, **3**(5): 1-16.

DeMets C, Gordon R G, Argus D F, Stein S. 1994. Effect of recent revisions to the geomagnetic reversal time scale on estimates of current plate motions. *Geophysical Research Letters*, **21**(20): 2 191-2 194.

Douville É, Charlou J L, Donval J P, Hureau D, Appriou P. 1999. Le comportement de l'arsenic (As) et de l'antimoine (Sb) dans les fluides provenant de différents systèmes hydrothermaux océaniquesAs and Sb behaviour in fluids from various deep-sea hydrothermal systems. *Comptes Rendus de l'Académie des Sciences - Series IIA - Earth and Planetary Science*, **328**(2): 97-104.

Edwards K J, Glazer B T, Rouxel O J, Bach W, Emerson D, Davis R E, Toner B M, Chan C S, Tebo B M, Staudigel H,

Moyer C L. 2011. Ultra-diffuse hydrothermal venting supports Fe-oxidizing bacteria and massive umber deposition at 5000 m off Hawaii. *ISME Journal*, **5**(11): 1748-1758.

Eissen J P, Nohara M, Cotten J, Hirose K. 1994. North Fiji Basin basalts and their magma sources: part I. Incompatible element constraints. *Marine Geology*, **116**(1-2): 153-178.

Emerson D, Moyer C L. 2002. Neutrophilic Fe-oxidizing bacteria are abundant at the Loihi Seamount hydrothermal vents and play a major role in Fe oxide deposition. *Applied and Environmental Microbiology*, **68**(6): 3 085-3 093.

Fouquet Y, Knott R, Cambon P, Fallick A, Rickard D, Desbruyeres D. 1996. Formation of large sulfide mineral deposits along fast spreading ridges. Example from off-axial deposits at 12°43'N on the East Pacific Rise. *Earth and Planetary Science Letters*, **144**(1-2): 147-162.

Fouquet Y, Marcoux E. 1995. Lead isotope systematics in Pacific hydrothermal sulfide deposits. *Journal of Geophysical Research*: *Solid Earth*, **100**(B4): 6 025-6 040.

Fouquet Y, Von Stackelberg U, Charlou J L, Donval J P, Erzinger J, Foucher J P, Herzig P, Mühe R, Soakai S, Wiedicke M, Whitechurch H. 1991. Hydrothermal activity and metallogenesis in the Lau back-arc basin. *Nature*, **349**(6312): 778-781.

Gamo T, Okamura K, Charlou J L, Urabe T, Auzende J M, Ishibashi J, Shitashima K, Chiba H. 1997. Acidic and sulfate-rich hydrothermal fluids from the Manus back-arc basin, Papua New Guinea. *Geology*, **25**(2): 139-142.

Gannoun A, Burton K W, Parkinson I J, Alard O, Schiano P, Thomas L E. 2007. The scale and origin of the osmium isotope variations in mid-ocean ridge basalts. *Earth and Planetary Science Letters*, **259**(3-4): 541-556.

Gena K, Mizuta T, Ishiyama D, Urabe T. 2001. Acid-sulphate type alteration and mineralization in the DESMOS Caldera, Manus back-arc basin, Papua New Guinea. *Resource Geology*, **51**(1): 31-44.

Gente P, Auzende J M, Renard V, Fouquet Y, Bideau D. 1986. Detailed geological mapping by submersible of the East Pacific Rise axial graben near 13°N. *Earth and Planetary Science Letters*, **78**(2-3): 224-236.

Glasby G P, Notsu K. 2003. Submarine hydrothermal mineralization in the Okinawa Trough, SW of Japan: an overview. *Ore Geology Reviews*, **23**(3-4): 299-339.

Goodfellow W D, Franklin J M. 1993. Geology, mineralogy, and chemistry of sediment-hosted clastic massive sulfides in shallow cores, Middle Valley, northern Juan de Fuca Ridge. *Economic Geology*, **88**(8): 2 037-2 068.

Guo K, Zeng Z G, Chen S, Zhang Y X, Qi H Y, Ma Y. 2017. The influence of a subduction component on magmatism in the Okinawa Trough: evidence from thorium and related trace element ratios. *Journal of Asian Earth Sciences*, **145**: 205-216.

Guo K, Zhai S K, Wang X Y, Yu Z H, Lai Z Q, Chen S, Song Z J, Ma Y, Chen Z X, Li X H, Zeng Z G. 2018. The dynamics of the southern Okinawa Trough magmatic system: new insights from the microanalysis of the An contents, trace element concentrations and Sr isotopic compositions of plagioclase hosted in basalts and silicic rocks. *Chemical Geology*, **497**: 146-161.

Halbach P, Hansmann W, Köppel V, Pracejus B. 1997. Whole-rock and sulfide lead-isotope data from the hydrothermal JADE field in the Okinawa back-arc trough. *Mineralium Deposita*, **32**: 70-78.

Halbach P, Nakamura K, Wahsner M, Lange J, Sakai H, Käselitz L, Hansen R D, Yamano M, Post J, Prause B, Seifert R, Michaelis W, Teichmann F, Kinoshita M, Märten A, Ishibashi J, Czerwinski S, Blum N. 1989. Probable modern analogue of Kuroko-type massive sulphide deposits in the Okinawa Trough back-arc basin. *Nature*, **338**(6215): 496-499.

Hannington M D, de Ronde C E J, Petersen S. 2005. Sea-floor tectonics and submarine hydrothermal systems. *In*: Economic Geology, 100th Anniversary Volume. Society of Economic Geologists Inc., Littleton, CO. p.111-114.

Harvey J, Gannoun A, Burton K W, Rogers N W, Alard O, Parkinson I J. 2006. Ancient melt extraction from the oceanic upper mantle revealed by Re-Os isotopes in abyssal peridotites from the Mid-Atlantic ridge. *Earth and Planetary Science Letters*, **244**(3-4): 606-621.

Hegner E, Tatsumoto M. 1987. Pb, Sr, and Nd isotopes in basalts and sulfides from the Juan de Fuca Ridge. *Journal of Geophysical Research*: *Solid Earth*, **92**(B11): 11 380-11 386.

Hékinian R, Francheteau J, Renard V, Ballard R D, Choukroune P, Cheminee J L, Albarede F, Minster J F, Charlou J L, Marty J C, Boulegue J. 1983. Intense hydrothermal activity at the axis of the East Pacific Rise near 13°N: sumbersible witnesses the growth of sulfide chimney. *Marine Geophysical Research*, **6**: 1-14.

Hrischeva E, Scott S D, Weston R. 2007. Metalliferous sediments associated with presently forming volcanogenic massive sulfides: the SuSu knolls hydrothermal field, Eastern Manus Basin, Papua New Guinea. *Economic Geology*, **102**(1): 55-73.

Huang P, Li A C, Hu N J, Fu Y T, Ma Z B. 2006. Isotopic feature and uranium dating of the volcanic rocks in the Okinawa Trough. *Science in China Series D*, **49**(4): 375-383.

Huang X, Chen S, Zeng Z G, Pu X Q, Hou Q H. 2017a. The influence of seafloor hydrothermal activity on major and trace elements of the sediments from the South Mid-Atlantic Ridge. *Journal of Ocean University of China*, **16**(5): 775-780, https://doi.org/10.1007/s11802-017-3311-y.

Huang X, Chen S, Zeng Z G, Pu X Q, Hou Q H. 2017b. Characteristics of hydrocarbons in sediment core samples from the northern Okinawa Trough. *Marine Pollution Bulletin*, **115**(1-2): 507-514.

Huang X, Zeng Z G, Chen S, Yin X B, Wang X Y, Ma Y, Yang B J, Rong G B, Shu Y C, Jiang T. 2014. Component characteristics of polycyclic aromatic compounds in sediments of the South Mid-Atlantic Ridge. *Acta Oceanologica Sinica*, **33**(11): 150-154.

Huang X, Zeng Z G, Chen S, Yin X B, Wang X Y, Zhao H J, Yang B J, Rong K B, Ma Y. 2013. Component characteristics of organic matter in hydrothermal barnacle shells from Southwest Indian Ridge. *Acta Oceanologica Sinica*, **32**(12): 60-67.

Humphris S E, Klein F. 2018. Progress in deciphering the controls on the geochemistry of fluids in seafloor hydrothermal systems. *Annual Review of Marine Science*, **10**: 315-343.

Ishibashi J I, Ikegami F, Tsuji T, Urabe T. 2015. Hydrothermal activity in the Okinawa Trough back-arc basin: geological background and hydrothermal mineralization. *In*: Ishibashi J I, Okino K, Sunamura M eds. Subseafloor Biosphere Linked to Hydrothermal Systems: TAIGA Concept. Springer, Tokyo. p.337-359, https://doi.org/10.1007/978-4-431-54865-2_27.

Kim J, Lee I, Halbach P, Lee K Y, Ko Y T, Kim K H. 2006. Formation of hydrothermal vents in the North Fiji Basin: sulfur and lead isotope constraints. *Chemical Geology*, **233**(3-4): 257-275.

Kim J, Lee I, Lee K Y. 2004. S, Sr, and Pb isotopic systematics of hydrothermal chimney precipitates from the Eastern Manus Basin, western Pacific: evaluation of magmatic contribution to hydrothermal system. *Journal of Geophysical Research*: *Solid Earth*, **109**(B12): B12210, https://doi.org/10.1029/2003JB002912.

Kishida K, Sohrin Y, Okamura K, Ishibashi J I. 2004. Tungsten enriched in submarine hydrothermal fluids. *Earth and Planetary Science Letters*, **222**(3-4): 819-827.

Koschinsky A, Seifert R, Halbach P, Bau M, Brasse S, de Carvalho L M, Fonseca N M. 2002. Geochemistry of diffuse low-temperature hydrothermal fluids in the North Fiji Basin. *Geochimica et Cosmochimica Acta*, **66**(8): 1 409-1 427.

Kuo F W. 2001. Preliminary Investigation of Shallow Hydrothermal Vents on Kueishantao Islet of Northeastern Taiwan. Institute of Marine Geology and Chemistry, National Sun Yat-Sen University, Kaohsiung, Taiwan. 81 pp. (in Chinese).

Kusakabe M, Mayeda S, Nakamura E. 1990. S, O and Sr isotope systematics of active vent materials from the Mariana backarc basin spreading axis at 18°N. *Earth and Planetary Science Letters*, **100**(1-3): 275-282.

LeHuray A P, Church S E, Koski R A, Bouse R M. 1988. Pb isotopes in sulfides from mid-ocean ridge hydrothermal sites. *Geology*, **16**(4): 362-365.

Lein A Y, Peresypkin V I, Simoneit B R T. 2003. Origin of hydrocarbons in hydrothermal sulfide ores in the Mid-Atlantic Ridge. *Lithology and Mineral Resources*, **38**(5): 383-393.

Liang W D, Tang T Y, Yang Y J, Ko M T, Chuang W S. 2003. Upper-ocean currents around Taiwan. *Deep Sea Research Part II*: *Topical Studies in Oceanography*, **50**(6-7): 1 085-1 105.

Liao S L, Tao C H, Zhu C W, Li H M, Li X H, Liang J, Yang W F, Wang Y J. 2019. Two episodes of sulfide mineralization at the Yuhuang-1 hydrothermal field on the Southwest Indian Ridge: insight from Zn isotopes. *Chemical Geology*, **507**: 54-63.

Metz S, Trefry J H. 2000. Chemical and mineralogical influences on concentrations of trace metals in hydrothermal fluids. *Geochimica et Cosmochimica Acta*, **64**(13): 2 267-2 279.

Mills R A, Elderfield H. 1995. Rare earth element geochemistry of hydrothermal deposits from the active TAG mound, 26°N Mid-Atlantic Ridge. *Geochimica et Cosmochimica Acta*, **59**(17): 3 511-3 524, https://doi.org/10.1016/0016-7037(95)00224-N.

Muller M R, Minshull T A, White R S. 1999. Segmentation and melt supply at the Southwest Indian Ridge. *Geology*, **27**(10): 867-870.

Nakamura K, Morishita T, Bach W, Klein F, Hara K, Okino K, Takai K, Kumagai H. 2009. Serpentinized troctolites exposed near the Kairei Hydrothermal Field, Central Indian Ridge: insights into the origin of the Kairei hydrothermal fluid supporting a unique microbial ecosystem. *Earth and Planetary Science Letters*, **280**(1-4): 128-136.

Nohara M, Hirose K, Eissen J P, Urabe T, Joshima M. 1994. The North Fiji Basin basalts and their magma sources: part II. Sr–Nd isotopic and trace element constraints. *Marine Geology*, **116**(1-2): 179-195.

Park S H, Lee S M, Kamenov G D, Kwon S T, Lee K Y. 2010. Tracing the origin of subduction components beneath the South East rift in the Manus Basin, Papua New Guinea. *Chemical Geology*, **269**(3-4): 339-349.

Petersen S, Herzig P M, Kuhn T, Franz L, Hannington M D, Monecke T, Gemmell J B. 2005. Shallow drilling of seafloor hydrothermal systems using the BGS rockdrill: conical seamount (New Ireland fore-arc) and PACMANUS (Eastern Manus Basin), Papua New Guinea. *Marine Georesources & Geotechnology*, **23**(3): 175-193.

Petersen S, Kuhn K, Kuhn T, Augustin N, Hékinian R, Franz L, Borowski C. 2009. The geological setting of the ultramafic-hosted Logatchev hydrothermal field (14°45′N, Mid-Atlantic Ridge) and its influence on massive sulfide formation. *Lithos*, **112**(1-2): 40-56.

Petersen S, Monecke T, Westhues A, Hannington M D, Gemmell J B, Sharpe R, Peters M, Strauss H, Lackschewitz K, Augustin N, Gibson H, Kleeberg R. 2014. Drilling shallow-water massive sulfides at the Palinuro volcanic complex, Aeolian island arc, Italy. *Economic Geology*, **109**(8): 2 129-2 158.

Peucker-Ehrenbrink B, Ravizza G. 2000. The marine osmium isotope record. *Terra Nova*, **12**(5): 205-219.

Pichler T, Veizer J. 1999. Precipitation of Fe(III) oxyhydroxide deposits from shallow-water hydrothermal fluids in Tutum Bay, Ambitle Island, Papua New Guinea. *Chemical Geology*, **162**(1): 15-31.

Rees C E, Jenkins W J, Monster J. 1978. The sulphur isotopic composition of ocean water sulphate. *Geochimica et Cosmochimica Acta*, **42**(4): 377-381.

Rong K B, Zeng Z G, Yin X B, Chen S, Wang X Y, Qi H Y, Ma Y. 2018. Smectite formation in metalliferous sediments

near the East Pacific Rise at 13°N. *Acta Oceanologica Sinica*, **37**(9): 67-81.

Rouxel O, Fouquet Y, Ludden J N. 2004. Copper isotope systematics of the Lucky Strike, Rainbow, and Logatchev sea-floor hydrothermal fields on the Mid-Atlantic Ridge. *Economic Geology*, **99**(3): 585-600.

Rouxel O, Shanks III W C, Bach W, Edwards K J. 2008. Integrated Fe- and S-isotope study of seafloor hydrothermal vents at East Pacific rise 9-10°N. *Chemical Geology*, **252**(3-4): 214-227.

Sakai H, Des Marais D, Ueda A, Moore J G. 1984. Concentrations and isotope ratios of carbon, nitrogen and sulfur in ocean-floor basalts. *Geochimica et Cosmochimica Acta*, **48**(12): 2 433-2 441.

Schiano P, Birck J L, Allègre C J. 1997. Osmium-strontium-neodymium-lead isotopic covariations in mid-ocean ridge basalt glasses and the heterogeneity of the upper mantle. *Earth and Planetary Science Letters*, **150**(3-4): 363-379.

Seyfried Jr W E, Pester N J, Tutolo B M, Ding K. 2015. The Lost City hydrothermal system: constraints imposed by vent fluid chemistry and reaction path models on subseafloor heat and mass transfer processes. *Geochimica et Cosmochimica Acta*, **163**: 59-79.

Shanks III W C, Seyfried Jr W E. 1987. Stable isotope studies of vent fluids and chimney minerals, southern Juan de Fuca Ridge: sodium metasomatism and seawater sulfate reduction. *Journal of Geophysical Research*: *Solid Earth*, **92**(B11): 11 387-11 399.

Sharma M, Rosenberg E J, Butterfield D A. 2007. Search for the proverbial mantle osmium sources to the oceans: hydrothermal alteration of mid-ocean ridge basalt. *Geochimica et Cosmochimica Acta*, **71**(19): 4 655-4 667.

Sharma M, Wasserburg G J, Hofmann A W, Butterfield D A. 2000. Osmium isotopes in hydrothermal fluids from the Juan de Fuca Ridge. *Earth and Planetary Science Letters*, **179**(1): 139-152.

Shinjo R, Kato Y. 2000. Geochemical constraints on the origin of bimodal magmatism at the Okinawa Trough, an incipient back-arc basin. *Lithos*, **54**(3-4): 117-137.

Shu Y C, Nielsen S, Zeng Z G, Shinjo R, Blusztajn J, Wang X Y, Chen S. 2017. Tracing subducted sediment inputs to the Ryukyu arc-Okinawa Trough system: evidence from thallium isotopes. *Geochimica et Cosmochimica Acta*, **217**: 462-491, https://doi.org/10.1016/j.gca.2017.08.035.

Sibuet J C, Deffontaines B, Hsu S K, Thareau N, Le Formal J P, Liu C SParty. 1998. Okinawa Trough backarc basin: early tectonic and magmatic evolution. *Journal of Geophysical Research*: *Solid Earth*, **103**(B12): 30 245-30 267.

Simoneit B R T, Lein A Y, Peresypkin V I, Osipov G A. 2004. Composition and origin of hydrothermal petroleum and associated lipids in the sulfide deposits of the Rainbow Field (Mid-Atlantic Ridge at 36°N). *Geochimica et Cosmochimica Acta*, **68** (10): 2 275-2 294.

Sinton J M, Ford L L, Chappell B, McCulloch M T. 2003. Magma genesis and mantle heterogeneity in the Manus back-arc basin, Papua New Guinea. *Journal of Petrology*,

44(1): 159-195.

Snow J E, Reisberg L. 1995. Os isotopic systematics of the MORB mantle: results from altered abyssal peridotites. *Earth and Planetary Science Letters*, **133**(3-4): 411-421.

Stuart F M, Ellam R M, Duckworth R C. 1999. Metal sources in the Middle Valley massive sulphide deposit, northern Juan de Fuca Ridge: Pb isotope constraints. *Chemical Geology*, **153**(1-4): 213-225.

Suo Y H, Li S Z, Li X Y, Zhang Z, Ding D. 2017. The potential hydrothermal systems unexplored in the Southwest Indian Ocean. *Marine Geophysical Research*, **38**(1-2): 61-70.

Suzuki R, Ishibashi J I, Nakaseama M, Konno U, Tsunogai U, Gena K, Chiba H. 2008. Diverse range of mineralization induced by phase separation of hydrothermal fluid: case study of the Yonaguni Knoll IV hydrothermal field in the Okinawa Trough Back-arc Basin. *Resource Geology*, **58**(3): 267-288.

Tao C H, Li H M, Jin X B, Zhou J P, Wu T, He Y H, Deng X M, Gu C H, Zhang G Y, Liu W Y. 2014. Seafloor hydrothermal activity and polymetallic sulfide exploration on the southwest Indian ridge. *Chinese Science Bulletin*, **59**(19): 2 266-2 276.

Tao C H, Seyfried Jr W E, Lowell R P, Liu Y L, Liang J, Guo Z K, Ding K, Zhang H T, Liu J, Qiu L, Egorov I, Liao S L, Zhao M H, Zhou J P, Deng X M, Li H M, Wang H C, Cai W, Zhang G Y, Zhou H W, Lin J, Li W. 2020. Deep high-temperature hydrothermal circulation in a detachment faulting system on the ultra-slow spreading ridge. *Nature Communications*, **11**: 1300.

Tarasov V G, Gebruk A V, Mironov A N, Moskalev L I. 2005. Deep-sea and shallow-water hydrothermal vent communities: two different phenomena? *Chemical Geology*, **224**(1-3): 5-39.

Tivey M K. 2007. Generation of seafloor hydrothermal vent fluids and associated mineral deposits. *Oceanography*, **20**(1): 50-65.

Verati C, Lancelot J, Hékinian R. 1999. Pb isotope study of black-smokers and basalts from Pito Seamount site (Easter microplate). *Chemical Geology*, **155**(1-2): 45-63.

Vidal P, Clauer N. 1981. Pb and Sr isotopic systematics of some basalts and sulfides from the East Pacific Rise at 21°N (project RITA). *Earth and Planetary Science Letters*, **55**(2): 237-246.

Von Damm K L. 1995. Temporal and compositional diversity in seafloor hydrothermal fluids. *Reviews of Geophysics*, **33**(S2): 1 297-1 305.

Wang X Y, Zeng Z G, Chen S, Yin X B, Chen C T A. 2013b. Rare earth elements in hydrothermal fluids from Kueishantao, off northeastern Taiwan: indicators of shallow-water, sub-seafloor hydrothermal processes. *Chinese Science Bulletin*, **58**(32): 4 012-4 020, https://doi.org/10.1007/s11434-013-5849-4.

Wang X Y, Zhao H J, Zeng Z G, Yin X B, Chen S, Ma Y. 2013a. Characteristics of silicon and oxygen isotopic compositions of basalts near East Pacific Rise 13°N. *Acta Oceanologica Sinica*, **32**(12): 104-108.

Woodruff L G, Shanks III W C. 1988. Sulfur isotope study of

chimney minerals and vent fluids from 21°N, East Pacific Rise: hydrothermal sulfur sources and disequilibrium sulfate reduction. *Journal of Geophysical Research*: *Solid Earth*, **93**(B5): 4 562-4 572.

Yamano M, Uyeda S, Foucher J P, Sibuet J C. 1989. Heat flow anomaly in the middle Okinawa Trough. *Tectonophysics*, **159**(3-4): 307-318.

Yang B J, Zeng Z G, Qi H Y, Wang X Y, Ma Y, Rong K B. 2015. Constraints on biotic and abiotic role in the formation of Fe-Si oxides from the PACMANUS Hydrothermal Field. *Ocean Science Journal*, **50**(4): 751-761.

Yao H Q, Zhou H Y, Peng X T, Bao S X, Wu Z J, Li J T, Sun Z L, Chen Z Q, Li J W, Chen G Q. 2009. Metal sources of black smoker chimneys, Endeavour Segment, Juan de Fuca Ridge: Pb isotope constraints. *Applied Geochemistry*, **24**(10): 1 971-1 977.

Zeng Z G, Chen C T A, Yin X B, Zhang X Y, Wang X Y, Zhang G L, Wang X M, Chen D G. 2011. Origin of native sulfur ball from the Kueishantao hydrothermal field offshore northeast Taiwan: evidence from trace and rare earth element composition. *Journal of Asian Earth Sciences*, **40**(2): 661-671.

Zeng Z G, Chen D G, Yin X B, Wang X Y, Zhang G L, Wang X M. 2010b. Elemental and isotopic compositions of the hydrothermal sulfide on the East Pacific Rise near 13ºN. *Science China Earth Sciences*, **53**(2): 253-266.

Zeng Z G, Chen S, Ma Y, Yin X B, Wang X Y, Zhang S P, Zhang J L, Wu X W, Li Y, Dong D, Xiao N. 2017a. Chemical compositions of mussels and clams from the Tangyin and Yonaguni Knoll IV hydrothermal fields in the southwestern Okinawa Trough. *Ore Geology Reviews*, **87**: 172-191,https://doi.org/10.1016/j.oregeorev.2016.09.015.

Zeng Z G, Chen S, Selby D, Yin X B, Wang X Y. 2014a. Rhenium-osmium abundance and isotopic compositions of massive sulfides from modern deep-sea hydrothermal systems: implications for vent associated ore forming processes. *Earth and Planetary Science Letters*, **396**: 223-234.

Zeng Z G, Chen S, Wang X Y, Ouyang H G, Yin X B, Li Z X. 2012c. Mineralogical and micromorphological characteristics of Si-Fe-Mn oxyhydroxides from the PACMANUS hydrothermal field, Eastern Manus Basin. *Science China Earth Sciences*, **55**(12): 2 039-2 048.

Zeng Z G, Jiang F Q, Zhai S K, Qin Y S. 2000. Lead isotopic compositions of massive sulfides from the Jade hydrothermal field in the Okinawa Trough and its geological implications. *Geochimica*, **29**(3): 239-245. (in Chinese with English abstract)

Zeng Z G, Liu C H, Chen C T A, Yin Y B, Chen D G, Wang X Y, Wang X M, Zhang G L. 2007. Origin of a native sulfur chimney in the Kueishantao hydrothermal field, offshore northeast Taiwan. *Science in China Series D*: *Earth Sciences*, **50**(11): 1 746-1 753.

Zeng Z G, Ma Y, Chen S, Selby D, Wang X Y, Yin X B. 2017b. Sulfur and lead isotopic compositions of massive sulfides from deep-sea hydrothermal systems: implications for ore genesis and fluid circulation. *Ore Geology Reviews*, **87**:

155-171,https://doi.org/10.1016/j.oregeorev.2016.10.014.

Zeng Z G, Ma Y, Wang X Y, Chen C T A, Yin X B, Zhang S P, Zhang J L, Jiang W. 2018c. Elemental compositions of crab and snail shells from the Kueishantao hydrothermal field in the southwestern Okinawa Trough. *Journal of Marine Systems*, **180**: 90-101, https://doi.org/10.1016/j.jmarsys.2016.08.012.

Zeng Z G, Ma Y, Yin X B, Selby D, Kong F C, Chen S. 2015b. Factors affecting the rare earth element compositions in massive sulfides from deep-sea hydrothermal systems. *Geochemistry*, *Geophysics*, *Geosystems*, **16**(8): 2 679-2 693, https://doi.org/10.1002/2015GC005812.

Zeng Z G, Niedermann S, Chen S, Wang X Y, Li Z X. 2015a. Noble gases in sulfide deposits of modern deep-sea hydrothermal systems: implications for heat fluxes and hydrothermal fluid processes. *Chemical Geology*, **409**: 1-11.

Zeng Z G, Ouyang H G, Yin X B, Chen S, Wang X Y, Wu L. 2012a. Formation of Fe-Si-Mn oxyhydroxides at the PACMANUS hydrothermal field, Eastern Manus Basin: mineralogical and geochemical evidence. *Journal of Asian Earth Sciences*, **60**: 130-146.

Zeng Z G, Qi H Y, Chen S, Yin X B, Li Z X. 2014b. Hydrothermal alteration of plagioclase microphenocrysts and glass in basalts from the East Pacific Rise near 13°N: an SEM-EDS study. *Science China Earth Sciences*, **57**(7): 1 427-1 437.

Zeng Z G, Qin Y S, Zhai S K. 2001. He, Ne and Ar isotope compositions of fluid inclusions in hydrothermal sulfides from the TAG hydrothermal field Mid-Atlantic Ridge. *Science in China Series D*: *Earth Sciences*, **44**(3): 221-228.

Zeng Z G, Qin Y S, Zhai S K. 2004. He, Ne and Ar isotope compositions of fluid inclusions in massive sulfides from the Jade hydrothermal field, Okinawa Trough. *Acta Oceanologica Sinica*, **25**(4): 36-42. (in Chinese with English abstract)

Zeng Z G, Wang Q Y, Wang X M, Chen S, Yin X B, Li Z X. 2012b. Geochemistry of abyssal peridotites from the super slow-spreading Southwest Indian Ridge near 65°E: implications for magma source and seawater alteration. *Journal of Earth System Science*, **121**(5): 1 317-1 336.

Zeng Z G, Wang X Y, Chen C T A, Qi H Y. 2018a. Understanding the compositional variability of the major components of hydrothermal plumes in the Okinawa Trough. *Geofluids*, **2018**: 1536352, https://doi.org/10.1155/2018/1536352.

Zeng Z G, Wang X Y, Chen C T A, Yin X B, Chen S, Ma Y Q, Xiao Y K. 2013. Boron isotope compositions of fluids and plumes from the Kueishantao hydrothermal field off northeastern Taiwan: implications for fluid origin and hydrothermal processes. *Marine Chemistry*, **157**: 59-66.

Zeng Z G, Wang X Y, Qi H Y, Zhu B W. 2018b. Arsenic and antimony in hydrothermal plumes from the eastern Manus basin, Papua New Guinea. *Geofluids*, **2018**: 6079586, https://doi.org/10.1155/2018/6079586.

Zeng Z G, Wang X Y, Zhang G L, Yin X B, Chen D G, Wang X M. 2008. Formation of Fe-oxyhydroxides from the East

Pacific Rise near latitude 13°N: evidence from mineralogical and geochemical data. *Science in China Series D: Earth Sciences*, **51**(2): 206-215.

Zeng Z G, Yu S X, Wang X Y, Fu Y T, Yin X B, Zhang G L, Wang X M, Chen S. 2010a. Geochemical and isotopic characteristics of volcanic rocks from the northern East China Sea shelf margin and the Okinawa Trough. *Acta Oceanologica Sinica*, **29**(4): 48-61, https://doi.org/10.1007/s13131-010-0050-y.

Zeng Z G, Yu S X, Yin X B, Wang X Y, Zhang G L, Wang X M, Chen D G. 2009. Element enrichment and U-series isotopic characteristics of the hydrothermal sulfides at Jade site in the Okinawa Trough. *Science in China Series D: Earth Sciences*, **52**(7): 913-924.

Zeng Z G. 2011. Submarine Hydrothermal Geology. Science Press, Beijing. 567p. (in Chinese)

Zhang W, Zeng Z G, Cui L K, Yin X B. 2018c. Geochemical constrains on MORB composition and magma sources at East Pacific Rise between 1°S and 2°S. *Journal of Ocean University of China*, **17**(2): 297-304.

Zhang Y X, Zeng Z G, Chen S, Wang X Y, Yin X B. 2018a. New insights into the origin of the bimodal volcanism in the middle Okinawa Trough: not a basalt-rhyolite differentiation process. *Frontiers of Earth Science*, **12**(2): 325-338, https://doi.org/10.1007/s11707-017-0638-z.

Zhang Y X, Zeng Z G, Li X H, Yin X B, Wang X Y, Chen S. 2018d. High-potassium volcanic rocks from the Okinawa Trough: implications for a cryptic potassium-rich and DUPAL-like source. *Geological Journal*, **53**(5): 1 755-1 766, https://doi.org/10.1002/gj.3000.

Zhang Y X, Zeng Z G, Qi H Y, Yin X B, Li H, Wang X Y, Chen S. 2018b. Two-stage influences of hydrothermal fluids on pumice near the Iheya North hydrothermal field, Okinawa Trough. *Marine Georesources & Geotechnology*, **36**(4): 393-404, https://doi.org/10.1080/1064119X.2017.1318987.

Zhang Y X, Zeng Z G, Wang X Y, Chen S, Yin X B. 2020. Factors controlling the geochemical differences between two types of rhyolites in the middle Okinawa Trough. *Geosciences Journal*, **24**(1): 35-48, https://doi.org/10.1007/s12303-018-0084-2.

Zierenberg R A, Koski R A, Morton J L, Bouse R M. 1993. Genesis of massive sulfide deposits on a sediment-covered spreading center, Escanaba Trough, Southern Gorda Ridge. *Economic Geology*, **88**(8): 2 069-2 098.